Astronomy & Astrophysics manuscript no. RKTM10
July 1, 2010

Quantifying the uncertainties of chemical evolution studies

II. Stellar yields

D. Romano[1,2], A. I. Karakas[3], M. Tosi[2], and F. Matteucci[4,5]

[1] Dipartimento di Astronomia, Università di Bologna, Via Ranzani 1, I-40127 Bologna, Italy
e-mail: donatella.romano@oabo.inaf.it
[2] INAF, Osservatorio Astronomico di Bologna, Via Ranzani 1, I-40127 Bologna, Italy
e-mail: monica.tosi@oabo.inaf.it
[3] Research School of Astronomy and Astrophysics, Mt. Stromlo Observatory, Cotter Rd., Weston Creek, ACT 2611, Australia
e-mail: akarakas@mso.anu.edu.au
[4] Dipartimento di Fisica, Università di Trieste, Via Tiepolo 11, I-34143 Trieste, Italy
e-mail: matteucc@oats.inaf.it
[5] INAF, Osservatorio Astronomico di Trieste, Via Tiepolo 11, I-34143 Trieste, Italy

Received 23 March 2010; accepted 28 June 2010

ABSTRACT

Context. Galactic chemical evolution models are useful tools to interpret the large body of high-quality observational data on the chemical composition of stars and gas in galaxies which have become available in recent years.
Aims. This is the second paper of a series which aims at quantifying the uncertainties in chemical evolution model predictions related to the underlying model assumptions. Specifically, it deals with the uncertainties due to the choice of the stellar yields.
Methods. We adopt a widely used model for the chemical evolution of the Galaxy and test the effects of changing the stellar nucleosynthesis prescriptions on the predicted evolution of several chemical species. Up-to-date results from stellar evolutionary models are taken into account carefully.
Results. We find that, except for a handful of elements whose nucleosynthesis in stars is well understood by now, large uncertainties still affect the model predictions. This is especially true for the majority of the iron-peak elements, but also for much more abundant species such as carbon and nitrogen. The main causes of the mismatch we find among the outputs of different models assuming different stellar yields and among model predictions and observations are: (i) the adopted location of the mass cut in models of type II supernova explosions; (ii) the adopted strength and extent of hot bottom burning in models of asymptotic giant branch stars; (iii) the neglection of the effects of rotation on the chemical composition of the stellar surfaces; (iv) the adopted rates of mass loss and of (v) nuclear reactions, and (vi) the different treatments of convection.
Conclusions. Our results suggest that it is mandatory to include processes such as hot bottom burning in intermediate-mass stars and rotation in stars of all masses in accurate studies of stellar evolution and nucleosynthesis. In spite of their importance, both these processes still have to be better understood and characterized. As for massive stars, presupernova models computed with mass loss and rotation are available in the literature, but they still wait for a self-consistent coupling with the results of explosive nucleosynthesis computations.

Key words. Galaxy: abundances – Galaxy: evolution – nuclear reactions, nucleosynthesis, abundances

1. Introduction

A large, everexpanding body of high-quality observational data is available nowadays for our own Galaxy, as well as for a few nearby galaxies, concerning the detailed chemical properties of their interstellar medium (ISM) and stellar populations. This wealth of data can be interpreted in the framework of galactic chemical evolution (GCE) models. Even though GCE is not yet a well-sound astrophysical theory, it is still a powerful instrument to understand when and how a given system formed and evolved. In fact, as different chemical elements are produced on different time scales in different astrophysical sites, the behaviour of key abundance ratios for a given galactic region allows us to trace the chronology of events in that region. Abundance ratios as a function of time or metallicity also provide important tests of possible nucleosynthesis scenarios (Tinsley 1979).

The main players in this game are the stellar yields, defined by Tinsley (1980) as the mass fractions of stars which are returned to the ISM in the form of newly produced elements during the entire stellar lifetimes. Following the pioneering works by Iben & Truran (1978) and Renzini & Voli (1981) for low- and intermediate-mass stars (LIMSs), and Arnett (1978) and Chiosi & Caimmi (1979) for massive stars, stellar models with an increasingly improved treatment of the relevant physical processes have appeared in the literature, thus providing different grids of yields. One of the most important differences among the various sets of yields is the presence of mass loss in massive star models. After Chiosi & Caimmi's (1979) paper, the most important work on yields from massive stars to include mass loss was from Maeder (1992). Maeder (1992) showed that mass loss driven by stellar winds mostly affects massive star models with solar or supersolar metallicities. In this case, stars lose large fractions of their newly produced helium and carbon. This has the effect of depressing the production of heavier elements, and in particular oxygen (see also

Dray et al. 2003; Dray & Tout 2003). This strong effect is particularly important in high metallicity environments such as the Galactic bulge (see McWilliam et al. 2008; Cescutti et al. 2009). In the following years the Geneva group has produced yields for massive stars with a lower mass loss rate than used previously by Maeder (1992), as well as the inclusion of stellar rotation (Meynet & Maeder 2002a; Hirschi et al. 2005; Hirschi 2007). The most significant result was the substantial quantity of primary N produced by including rotation in very-low metallicity massive star models (Hirschi 2005, 2007; Chiappini et al. 2006). Unfortunately, yields including mass loss through stellar winds are available only from a limited number of studies, whereas the majority of nucleosynthesis studies including a large number of chemical species do not include mass loss from massive stars. Among these we recall Woosley & Weaver (1995); Limongi & Chieffi (2003); Chieffi & Limongi (2004). The recent study by Kobayashi et al. (2006) includes mass loss but no rotation. Concerning LIMSs, nucleosynthesis yields including mass loss were from Renzini & Voli (1981), van den Hoek & Groenewegen (1997), Marigo (2001). More recently Karakas & Lattanzio (2007) and Karakas (2010) have provided metallicity dependent yields. Concerning type Ia supernovae (SNeIa, exploding white dwarfs in binary systems) the most commonly adopted yields are those from Nomoto et al. (1984, their model W7), subsequently revised by Iwamoto et al. (1999). These yields are preferred over others because they can very well reproduce the observed abundance pattern in SNIa ejecta. Empirical yields for massive stars and SNIa were derived by François et al. (2004), who modified the existing yields in order to reproduce the solar abundances and the [X/Fe][1] versus [Fe/H] patterns observed in the solar vicinity. Their yields mainly differ from the standard ones (in this case those of Woosley & Weaver 1995) for Mg, Si, and the Fe-peak elements. However, it should be noted that no computed yields can reproduce the abundance patterns of the Fe-peak elements in the solar vicinity.

The yields currently available for the most abundant elements result from updated stellar evolution and nucleosynthesis calculations, but differ quite significantly from each other. This implies that chemical evolution models assuming different yields can predict quite different element abundances even if they assume similar galactic parameters, such as the infall and star formation rate (SFR) or the initial mass function (IMF). It is therefore important to quantify what is the effect of different yields on the model results. To this purpose we compare stellar yields currently available in the literature and describe the corresponding differences in the outcome of a well tested chemical evolution model for our Galaxy.

The layout of the paper is as follows. In Sect. 2 we concisely review the prescriptions about the physical ingredients of the stellar models adopted by different authors. This provides the different yield sets explored in this study. A comparison between the different yield sets is also presented. In Sect. 3 we introduce the adopted GCE model. Our results are presented and compared with the corresponding observational data in Sects. 4 to 6. In Sect. 4 we deal with the evolution of elements from carbon to zinc in the solar neighbourhood. The Galactic abundance gradients are briefly discussed in Sect. 5. The helium variation with metallicity is analysed in Sect. 6. Sect. 7 summarizes and discusses the results.

[1] Throughout this paper, the standard notations [A/B] $\equiv \log (N_A/N_B) - \log(N_A/N_B)_\odot$ and $\log \varepsilon(A) \equiv \log(N_A/N_H)+12$ are used, where N_A, N_B and N_H are the number densities of elements A, B and hydrogen. Solar abundances are taken from Grevesse & Sauval (1998), unless otherwise specified.

2. Stellar yields

In this section we provide a detailed comparison between the different yield sets adopted in this work. The reader is referred to the source papers for a more thorough discussion of the adopted input physics.

For LIMSs (see Sect. 2.1), we consider the yields by: (i) van den Hoek & Groenewegen (1997), for two choices of the mass loss rate and minimum core mass for hot bottom burning; (ii) Marigo (2001), for two choices of the mixing-length parameter; (iii) Karakas & Lattanzio (2007) standard set, taking the contribution from 'extra pulses' into account, and (iv) Karakas (2010), who has recently recomputed Karakas & Lattanzio's (2007) models with updated nuclear reaction rates and enlarged the grid of masses and metallicities.

For massive stars (see Sect. 2.2), we consider the yields by: (i) Woosley & Weaver (1995), computed without mass loss and without rotation; (ii) Kobayashi et al. (2006), including metallicity-dependent mass loss, and (iii) the Geneva group (Meynet & Maeder 2002a; Hirschi et al. 2005; Hirschi 2007; Ekström et al. 2008), limited to the presupernova stage, but computed with both mass loss and rotation. Older yields by Maeder (1992) for solar-metallicity stars – with higher mass loss rates but without rotation – are considered as well. All of the adopted yield sets are metallicity dependent and are provided for various metallicities.

2.1. Low- and intermediate-mass stars

Stars with initial masses between ∼1 and ∼5–8 $M_\odot$ (depending on the overshooting adopted in the stellar evolutionary models) pass through a phase of double-shell burning, referred to as thermally-pulsing asymptotic giant branch (TP-AGB) phase, before ending their lives as white dwarfs. During the TP-AGB phase, they experience a number of thermal pulses followed by mixing episodes, the third dredge-up (TDU). In the most massive models, hot bottom burning (HBB) can occur if the base of the convective envelope is exposed to temperatures hot enough to trigger proton-capture nucleosynthesis. During the TP-AGB evolution, the stars experience a very rich nucleosynthesis whose products (most notably He, C, N, Na, Mg and *s*-process elements) are convected to the outermost layers and eventually injected into the ISM by stellar winds. These stars are hence important contributors to the chemical enrichment of galaxies.

van den Hoek & Groenewegen (1997) published yields of ^{4}He, ^{12}C, ^{13}C, ^{14}N and ^{16}O for stars with initial masses in the range 0.8–8 $M_\odot$ and initial compositions (Y, Z) = (0.243, 0.001), (0.252, 0.004), (0.264, 0.008), (0.30, 0.02) and (0.34, 0.04). They used the metallicity-dependent tracks provided by the Geneva group (e.g. Schaller et al. 1992) to follow the stellar evolution prior to the AGB phase, with the recipes outlined in Groenewegen & de Jong (1993) to include the effects of the first and second dredge-ups on the yields. Then, they followed the chemical evolution and mass loss up to the planetary nebula (PN) ejection with a synthetic TP-AGB evolution model. The effect of HBB was included in an approximate way and a Reimers (1975) law was assumed for the mass loss of stars on the AGB. These models do not consider any extra mixing. In this work we explore the van den Hoek & Groenewegen (1997) yield sets with mass loss scaling parameter along the AGB, η_{AGB}, either

varying with metallicity or constant. When the set with a constant $\eta_{\rm AGB}$ is assumed, we also investigate the effect of reducing the mass range in which HBB is allowed to occur.

Marigo (2001) followed the evolution of LIMSs with initial mass from ∼0.8 to 5 $M_\odot$ for three choices of the original composition, namely $(Y, Z) = (0.240, 0.004)$, $(0.250, 0.008)$ and $(0.273, 0.019)$. From the zero-age main sequence up to the onset of the TP-AGB phase, she has used complete stellar models by Girardi et al. (2000), including moderate core overshooting and external convection, but no extra mixing. Later phases have been treated with the help of synthetic TP-AGB models (Marigo et al. 1999). The classical Reimers (1975) formula has been used to include mass loss along the red giant branch (RGB), while mass loss during the TP-AGB phase has been included by means of the semi-empirical formalism developed by Vassiliadis & Wood (1993). Yields of ^{3}He, ^{4}He, ^{12}C, ^{13}C, ^{14}N, ^{15}N, ^{16}O, ^{17}O and ^{18}O are provided for three choices of the mixing-length parameter, namely $\alpha = 1.68$, 2.00 and 2.50. We investigate the effect of choosing the yields corresponding to either the lowest or the highest α value in Sect. 4.1.

The AGB yields of Karakas & Lattanzio (2007) and Karakas (2010) were calculated from detailed stellar models, where the structure was computed first and the nucleosynthesis calculated afterward using a post-processing algorithm. Yields are included for 77 nuclei including all stable isotopes from H to ^{34}S, and for a small group of Fe-peak nuclei. The details of this procedure and the codes used to compute the models have been previously described in some detail, see for example Karakas et al. (2009) and references therein. The models cover a range in mass from 1.0 $M_\odot$ to 6 $M_\odot$ and compositions $Z = 0.02$, 0.008, 0.004, and $Z = 0.0001$. All models were evolved from the zero-age main sequence to near the tip of the TP-AGB. The TDU efficiency governs the nucleosynthesis in the lower mass models; this was found to vary as a function of the H-exhausted core mass, metallicity, and envelope mass (see Karakas et al. 2002, for details). For example, in the $Z = 0.02$ models, no TDU was found for $m \leq 2$ $M_\odot$. For the intermediate-mass models, the TDU was found to be efficient and the o ccurrence of HBB also played a strong role in determining the final yields. The occurrence of HBB also depends on the initial mass and metallicity, with HBB occurring in lower mass stars with a decrease in metallicity (at 3 $M_\odot$ at $Z = 10^{-4}$, whereas it only starts at 5 $M_\odot$ at $Z = 0.02$). Furthermore, HBB is eventually shut down by the action of mass loss. For further details we refer to Karakas & Lattanzio (2007) and Karakas (2010). These models employ the mixing-length theory of convection with $\alpha = 1.75$. On the RGB Reimer's mass loss is adopted with $\eta_{\rm R} = 0.4$. On the AGB, Vassiliadis & Wood (1993) mass loss is used for all stellar models in Karakas & Lattanzio (2007) and most models in Karakas (2010); in Karakas (2010) Reimer's was used on the AGB for models between 3 to 6 $M_\odot$ with $Z = 10^{-4}$ (see reference for details). The main difference between the Karakas & Lattanzio (2007) models and those presented in Karakas (2010) is the choice of reaction rates used in the post-processing algorithm. Karakas (2010) used an updated set of proton and α-capture rates that include some of the latest experimental results for important reactions involved in the CNO cycle, and the NeNa and MgAl chains. Furthermore, Karakas (2010) assumed scaled-solar initial abundances for the $Z = 0.008$ and $Z = 0.004$ models: Karakas & Lattanzio (2007) adopted initial abundances for the Large and Small Magellanic Clouds from Russell & Dopita (1992) which are sub-solar for C, N, and O. The main difference between the yields of Karakas & Lattanzio (2007) and Karakas (2010) is that ∼6–30 times less Na is produced by intermediate-mass models with HBB. The yields of Karakas & Lattanzio (2007) also included the contribution from 'extra pulses', that is thermal pulses that were not computed using the detailed stellar evolution code but with the help of a synthetic TP-AGB model. This was done because it was not always possible to evolve the models to the tip of the AGB owing to convergence difficulties. If there was sufficient envelope mass left, further thermal pulses and TDU could potentially occur. In Karakas (2010), the contribution from these extra pulses was *not* included. This was because the synthetic AGB models required an assumption about the efficiency of the TDU for these last pulses. Full calculations have shown that the efficiency approaches zero as the envelope mass is decreased (Vassiliadis & Wood 1993; Straniero et al. 1997; Karakas et al. 2002). The new intermediate-mass $Z = 0.0001$ AGB models presented in Karakas (2010) were evolved to small envelope masses (∼0.1 $M_\odot$ in some cases). These models did not show any decrease in TDU efficiency with decreasing envelope mass, but in general low-metallicity models tend to experience more efficient mixing (e.g. Boothroyd & Sackmann 1988; Karakas et al. 2002).

2.2. Massive stars

Only a small fraction of the stellar mass, from 7 to 20 per cent, depending on the choice of the IMF (see Romano et al. 2005, hereinafter Paper I), is in stars with masses above 8 $M_\odot$. Nevertheless, these stars are major galactic polluters. They produce almost the whole body of the α and *r*-process elements and, if rotating fast, large amounts of primary ^{13}C, ^{14}N, ^{22}Ne and *s*-process elements at low metallicities (see Meynet et al. 2009, for a review on rotating high-mass stars). Massive stars are also thought to be the main factories of copper in galaxies (Romano & Matteucci 2007).

Woosley & Weaver (1995) provided the nucleosynthetic yields of isotopes lighter than $A = 66$ (zinc) for stars of various metallicities ($Z/Z_\odot = 0$, 0.0001, 0.01, 0.1 and 1) and masses in the range 11–40 $M_\odot$. In their models, each star is exploded using a piston to give a final kinetic energy of the ejecta at infinity of about 10^{51} ergs. The explosive modifications to the presupernova nucleosynthesis are computed by taking the effects of neutrino irradiation into account. Mass loss is not included in the presupernova models. Following the onset of a successful shock, stars more massive than 30 $M_\odot$ may experience considerable reimplosion of heavy elements. The amount of matter which falls back onto the collapsed remnant depends mainly on the initial energy of the explosion. For stars with $m \geq 30$ $M_\odot$, yields are given for different choices of the explosion energy (models labelled A, B, C in Woosley & Weaver 1995). We adopt both case A and case B, the latter corresponding to a slightly larger final kinetic energy of the ejecta at infinity (typically 1.9×10^{51} ergs rather than 1.2×10^{51} ergs). We systematically halve their Fe yields. This leads to a better fit to most of the observed abundance ratios (see Sect. 4). A factor of 2 of reduction is well within the uncertainties in modelling the explosion. Furthermore, the reduced Fe yields are consistent with observations of several type II supernovae (SNeII; Timmes et al. 1995).

It is now acknowledged that there exist two types of core-collapse SNe. One is normal SNeII (including Ib and Ic), with explosion energies of the order of 10^{51} ergs. The other is hypernovae (HNe), with more than 10 times larger explosion energies (Iwamoto et al. 1998). Kobayashi et al. (2006) have calculated the yields for both SNeII and HNe as functions of the initial

Table 1. Yields for massive stars from presupernova Geneva models including mass loss and rotation. Listed are: the initial metallicity of the stars, $Z_{\rm ini}$, the initial stellar masses (in $M_\odot$) and rotational velocities (in km s^{-1}), $m_{\rm ini}(\upsilon_{\rm ini})$, and the reference papers from which the yields have been picked up. See the text for details.

$Z_{\rm ini}$	$m_{\rm ini}(\upsilon_{\rm ini})$	Ref.
0	9(500), 15(800), 25(800), 40(800), 60(800), 85(800)	1
10^{-8}	9(500), 20(600), 40(700), 60(800), 85(800)	2
10^{-5}	9(300), 15(300), 20(300), 40(300), 60(300)	3
0.004	9(300), 12(300), 15(300), 20(300), 25(300), 40(300), 60(0)	3
0.02	12(300), 15(300), 20(300), 25(300), 40(300), 60(300)	4

References. (1) Ekström et al. (2008); (2) Hirschi (2007); (3) Meynet & Maeder (2002a); (4) Hirschi et al. (2005).

masses (from 13 to 40 $M_\odot$) and metallicities (Z = 0, 0.001, 0.004, 0.02) of the progenitor stars. Their calculations start on the main sequence and proceed through core collapse, with the inclusion of metallicity-dependent mass loss (de Jager et al. 1988; Kudritzki et al. 1989). The progenitor model is exploded when a central density of 3×10^{10} g cm^{-3} is reached. For SNeII, the final yields are obtained by setting the mass cut in such a way that 0.07 $M_\odot$ of Fe are ejected. For HNe, the final yields are obtained by adjusting the free parameters involved in the 'mixing and fallback' mechanism (Umeda & Nomoto 2002) to give [O/Fe] $\simeq$ 0.5 in the ejecta, as observed in extremely metal-poor stars. In order to include HN nucleosynthesis in GCE models, one should introduce a free parameter describing the fraction of HNe. In the present work, we analyze the two extreme cases where either none ($\varepsilon_{\rm HN}$ = 0) or all ($\varepsilon_{\rm HN}$ = 1) stars with $m \geq 20$ $M_\odot$ explode as HNe.

The inclusion of rotation in stellar evolutionary models considerably alters the outputs of traditional nucleosynthesis. Yields of ^{4}He, ^{12}C, ^{14}N and ^{16}O are available for high-mass rotating stars, for a fine grid of initial masses and metallicities (Meynet & Maeder 2002a; Hirschi et al. 2005; Hirschi 2007; Ekström et al. 2008, see Table 1). Yields of ^{13}C, ^{17}O and ^{18}O are provided only for a subset of models. The models include diffusion by shears, meridional circulation and mass loss and are computed up to the end of the C-burning phase. The absence of a proper, self-consistent computation of the nucleosynthesis occurring at the SN stage is the major shortcoming of such models. However, the presupernova yields of ^{4}He and CNO nuclei should be almost unaffected by subsequent explosive nucleosynthesis (e.g. Woosley & Weaver 1995) and can thus be safely used in GCE models. The grid of yields for high-mass rotators that we use in this study has been obtained by patching together results presented in different papers by the same group (see Table 1). We also test the models computed by Meynet & Maeder (2002a), Hirschi et al. (2005) and Ekström et al. (2008) for non-rotating high-mass stars (see Sect. 4.1).

2.3. Comparison among different yield sets

In the previous sections, we have considered a number of stellar evolution and nucleosynthesis studies. We have reviewed the basic input physics used in the stellar structure computations and schematically discussed the resulting yield sets. Other works on stellar evolution and nucleosynthesis exist in the literature besides the ones considered here, providing different grids of yields. However, these grids are computed either for mass/metallicity ranges smaller than the ones used here, or without the inclusion of some important physical processes affecting the final yields. Others are not much different from those considered here. The latter, for instance, is the case of the yields presented by Izzard et al. (2004), which are very similar to the ones by Karakas & Lattanzio (2007) (see figures from 2 to 7 of Karakas & Lattanzio 2007) and are thus not included in the present study. The Geneva group provides yields for LIMSs to be used to complete their grid of high-mass models. However, the computation of the LIMS models is stopped at the beginning of the TP-AGB phase. When dealing with LIMSs, the inclusion of the final nuclear burning phase is an essential step towards computing trustworthy yields of the CNO elements. Therefore, we prefer not to include the Geneva yields for LIMSs in our GCE models until they do cover the TP-AGB phase too. As a last example, Ventura & D'Antona (2008a,b) have recently provided new grids of yields for intermediate-mass stars for many chemical species. With the main goal of testing the self-enrichment scenario by massive AGB stars for Galactic globular clusters (see Ventura & D'Antona 2008a, and references therein), their prescriptions cover a relatively narrow range of initial stellar masses (3–6.5 $M_\odot$) and chemical compositions (Z = 0.001 and 0.004). As such, they are not suitable for use in chemical evolution models of the Milky Way and other systems where stars of all masses and metallicity have contributed to the enrichment.

The results from stellar nucleosynthesis are steadily improving with time, but we are still missing a complete and homogeneous set of stellar yields – the 'ideal grid' of yields computed with the same input physics for various initial masses and metallicities of the stars, spanning the whole range from 0.8 to 100 $M_\odot$ in initial stellar mass and from zero to (at least) twice solar in initial metallicity. Such an optimal yield set should also take into account all the relevant physical processes occurring in the stellar interiors and affecting the chemical composition of the ejected layers during the whole stellar lifetime (see Tosi 2007, for a recent appraisal of the problem).

The potential risks of patching together different yield sets are highlighted in Figs. 1 and 2 (see also Tosi 2007). The left-hand panels of Fig. 1 show the solar yields of van den Hoek & Groenewegen (1997) for LIMSs combined with those of Woosley & Weaver (1995) for massive stars (upper panel), the solar yields of Marigo (2001) for LIMSs combined with those of Maeder (1992) for He, C, N, O and Kobayashi et al. (2006) for all other elements from massive stars (middle panel) and the solar yields of Karakas (2010) for LIMSs combined with those of Hirschi et al. (2005) for He, C, N, O and Kobayashi et al. (2006) for all other elements from massive stars (lower panel). The Marigo (2001) yield set is completed with the homogeneous yields by Portinari et al. (1998) for stars of initial mass m = 6 $M_\odot$ and m = 7 $M_\odot$. Other combinations of yields

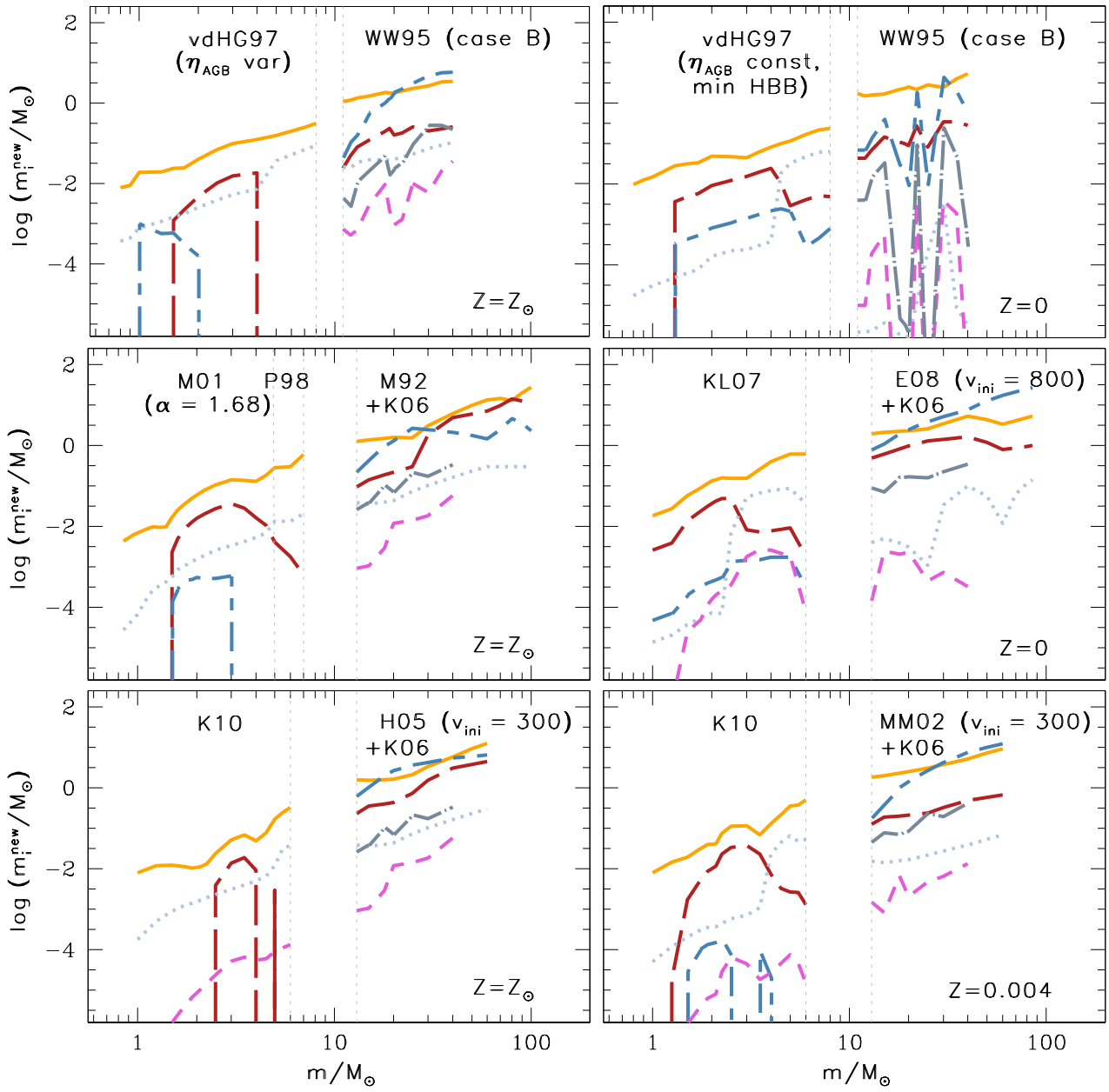

Fig. 1. Ejected masses of newly produced elements as a function of the stellar initial mass, from different authors (vdHG97: van den Hoek & Groenewegen 1997; WW95: Woosley & Weaver 1995; M01: Marigo 2001; P98: Portinari et al. 1998; M92: Maeder 1992; K06: Kobayashi et al. 2006; KL07: Karakas & Lattanzio 2007; E08: Ekström et al. 2008; K10: Karakas 2010; H05: Hirschi et al. 2005; MM02: Meynet & Maeder 2002a) and for different initial metallicities. Solid (orange) lines: He; long-dashed (red) lines: C; dotted (light blue) lines: N; short-dashed-long-dashed (blue) lines: O; short-dashed (magenta) lines: Na; dot-dashed (gray) lines: Mg. See the electronic edition of the journal for a colour version of this figure.

for different metallicities[2] are shown in the right-hand panels of Fig. 1.

Two problems are immediately apparent. First, a gap is present between the LIMS and high-mass star domains, from 8 to 11 M$_\odot$ or from 6 to 13 M$_\odot$, depending on the choice of the yield sets. This gap forces us to interpolate the yields over a non-negligible mass interval. This mass interval is the domain of the so-called super-AGB stars, that have not reliable nucleosynthetic output (Siess 2007; Pumo et al. 2008, and references therein). Moreover, as shown below, once weighted with the IMF this mass range is one of the major contributors to the Galactic enrichment. Second, several nucleosynthesis computations do not go beyond 40 M$_\odot$, which requires an uncertain extrapolation to higher masses. While, thanks to the negative slope of the IMF, this may be of little concern in modelling the recent chemical evolution of the Milky Way, it becomes extremely relevant for

[2] Since neither van den Hoek & Groenewegen (1997) nor Karakas & Lattanzio (2007) provide yields for zero-metallicity stars, at $Z = 0$ we adopt the yields corresponding to the lowest metallicities considered by those authors, namely $Z = 0.001$ for van den Hoek & Groenewegen (1997) and $Z = 0.0001$ for Karakas & Lattanzio (2007).

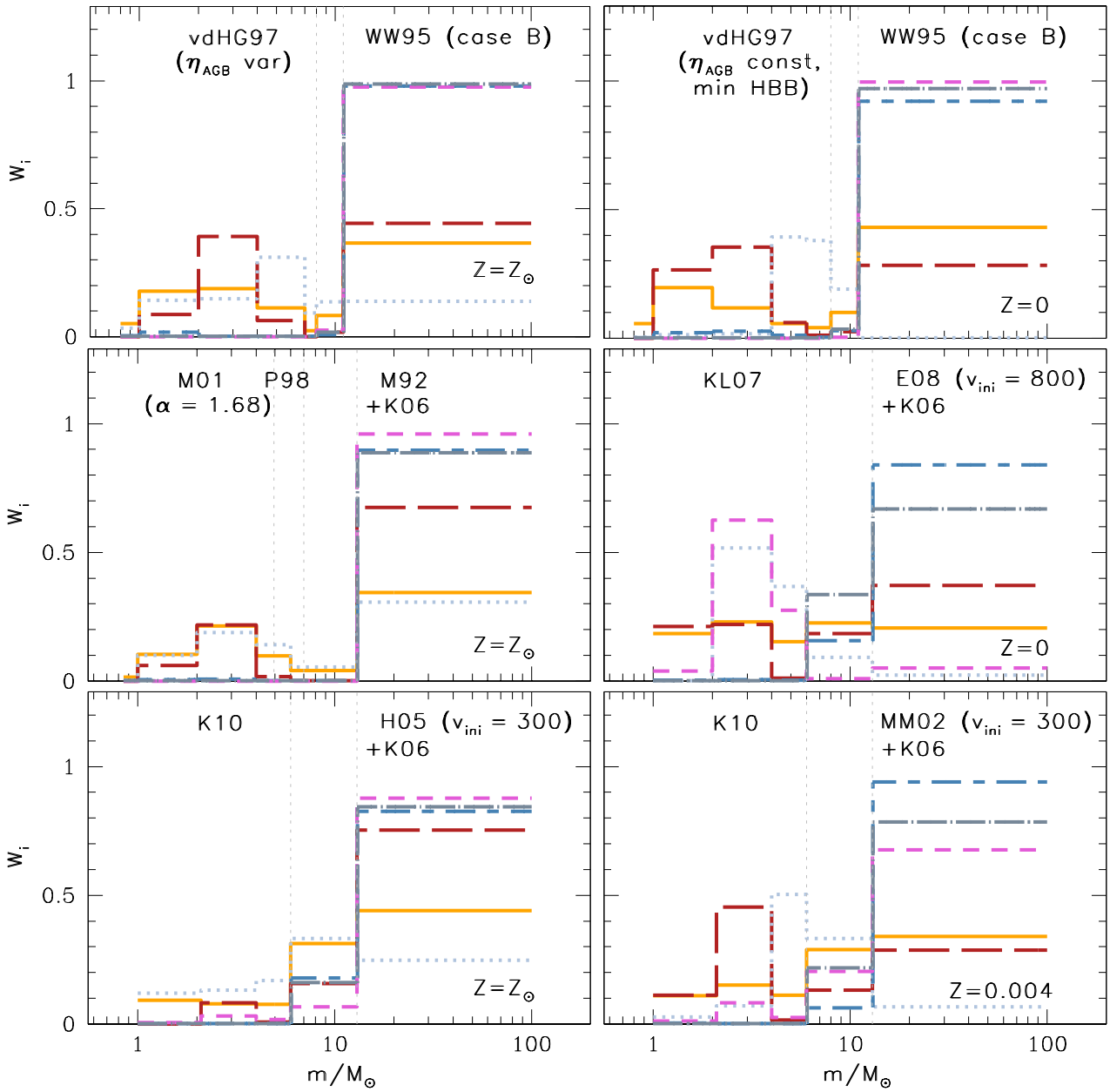

Fig. 2. IMF weighted yields in specific mass ranges. Line types and colours are the same as in Fig. 1. See the electronic edition of the journal for a colour version of this figure.

the very early epochs, when only the most massive stars were polluting the ISM.

To evaluate the contribution to the Galaxy enrichment of a given mass range, one must take the IMF into account. An efficient way to do that is to compute the IMF weighted yields. Let us first define for each element the integrated yield as:

$$P_i \equiv \int_{m_l}^{m_u} m_i^{\rm new}(m)\phi(m)dm, \quad (1)$$

where $m_l = 0.1$ M$_\odot$ and $m_u = 100$ M$_\odot$ are, respectively, the lower and upper mass limits to the mass range of all stars formed in the examined region; $m_i^{\rm new}(m)$ is the yield (in solar masses) and $\phi(m)$ is the IMF. The IMF weighted yield is:

$$W_i \equiv \frac{\int_{m_1}^{m_2} m_i^{\rm new}(m)\phi(m)dm}{P_i}, \quad (2)$$

where m_1 and m_2 are the lower and upper mass limits of the examined range.

In Fig. 2, the yields of Fig. 1 are weighted with the IMF of Kroupa et al. (1993). In computing the weighted yields, a linear interpolation is performed over the 8–11 M$_\odot$ (6–13 M$_\odot$, depending on the stellar models) mass range. When needed, the yields for massive stars are extrapolated to 100 M$_\odot$ by keeping constant the last computed masses ejected as newly produced elements. Very often, a bump is seen in the production of specific elements from stars in the 8–11 (6–13) M$_\odot$ interpolated mass range. In practice, more than 30% of all He and N newly produced by a stellar generation can come from stars in the 6–13 M$_\odot$ interval if the Karakas (2010)+Geneva+Kobayashi et al. (2006) combination of yields is adopted (Fig. 2, bottom panels). This enhanced contribution can be completely spurious.

Table 2. Nucleosynthesis prescriptions.

Model	Adopted stellar yields		Comments
	LIMSs	Massive stars	
1	vdHG97, $\eta_{\rm AGB}$ var	WW95, case B	Reference model
2	vdHG97, $\eta_{\rm AGB}$ var	WW95, case A	Mass cut changed
3	vdHG97, $\eta_{\rm AGB}$ var	WW95, case B + M92 pre-SN yields	Winds from $Z = Z_{\odot}$ massive stars included
4	vdHG97, $\eta_{\rm AGB}$ var	K06, $\varepsilon_{\rm HN} = 0$	SNII yields changed
5	vdHG97, $\eta_{\rm AGB}$ var	K06, $\varepsilon_{\rm HN} = 1$	HN nucleosynthesis included
6	vdHG97, $\eta_{\rm AGB}$ var	K06, $\varepsilon_{\rm HN} = 1$ + Geneva pre-SN yields, $\upsilon_{\rm ini} \neq 0$	Stellar rotation included
7	vdHG97, $\eta_{\rm AGB}$ var	K06, $\varepsilon_{\rm HN} = 1$ + Geneva pre-SN yields, $\upsilon_{\rm ini} = 0$	
8	vdHG97, $\eta_{\rm AGB}$ const	K06, $\varepsilon_{\rm HN} = 1$ + Geneva pre-SN yields, $\upsilon_{\rm ini} \neq 0$	Mass loss along the AGB changed
9	vdHG97, minimum HBB	K06, $\varepsilon_{\rm HN} = 1$ + Geneva pre-SN yields, $\upsilon_{\rm ini} \neq 0$	HBB extent reduced
10	M01, $\alpha = 1.68$	K06, $\varepsilon_{\rm HN} = 1$ + Geneva pre-SN yields, $\upsilon_{\rm ini} \neq 0$	LIMS yields changed
11	M01, $\alpha = 2.50$	K06, $\varepsilon_{\rm HN} = 1$ + Geneva pre-SN yields, $\upsilon_{\rm ini} \neq 0$	HBB strength increased
12	M01, $\alpha = 1.68$	K06, $\varepsilon_{\rm HN} = 1$ + [Geneva, $\upsilon_{\rm ini} \neq 0$ + M92] pre-SN yields	
13	KL07, with extra pulses	K06, $\varepsilon_{\rm HN} = 1$ + Geneva pre-SN yields, $\upsilon_{\rm ini} \neq 0$	AGB yields from detailed stellar models
14	KL07, with extra pulses	K06, $\varepsilon_{\rm HN} = 1$ + [Geneva, $\upsilon_{\rm ini} \neq 0$ + M92] pre-SN yields	
15	K10, without extra pulses	K06, $\varepsilon_{\rm HN} = 1$ + Geneva pre-SN yields, $\upsilon_{\rm ini} \neq 0$	Up-to-date nuclear reaction rates for LIMSs

Notes. vdHG97: van den Hoek & Groenewegen (1997); WW95: Woosley & Weaver (1995); M92: Maeder (1992); K06: Kobayashi et al. (2006); M01: Marigo (2001); KL07: Karakas & Lattanzio (2007); K10: Karakas (2010). The models adopting the yields by Marigo (2001) for LIMSs use self-consistent nucleosynthesis prescriptions from Portinari et al. (1998) for stars of initial mass $m = 6$ M$_{\odot}$ and $m = 7$ M$_{\odot}$.

The only way to overcome these problems is getting homogeneous and complete sets of yields.

3. The chemical evolution model

To compare the contribution to the Galaxy enrichment of the yields described in the previous sections, we adopt the *two-infall model* case B for the chemical evolution of the Galaxy. A thorough discussion of the adopted formalism and basic equations can be found elsewhere (Chiappini et al. 1997, 2001). Here we briefly recall the overall evolutionary scenario.

The inner halo and thick disc of the Milky Way are assumed to form on a relatively short time-scale (about 1 Gyr) out of a first infall episode, whereas the thin disc forms inside-out (Matteucci & François 1989) on longer time-scales (7 Gyr in the solar vicinity and more than a Hubble time at the outermost radii; see also Romano et al. 2000) during a second independent episode of extragalactic gas infall. The Galactic disc is approximated by several independent rings, 2 kpc wide. Radial flows are not considered here. Galactic outflows seem unlikely owing to the deep Galactic potential well, and are thus not included in the model. The adopted SFR is proportional to both the total mass and the gas surface densities. The efficiency of conversion of gas into stars is higher during the halo/thick-disc phase than during the thin-disc phase. Furthermore, it drops to zero every time the gas density drops below a critical density threshold. The instantaneous recycling approximation is relaxed, i.e. the stellar lifetimes are taken into account in details. As for the stellar IMF, the Kroupa et al. (1993) IMF is assumed (see Paper I, and further discussion in Sect. 6) in the 0.1–100 M$_{\odot}$ mass range. The rate of SNIa explosions is calculated as in Matteucci & Greggio (1986). SNeIa explode in close binary systems when a CO white dwarf has reached a critical mass limit because of accretion of hydrogen-rich matter from a main sequence or red giant companion.

The yields for SNeIa are taken from Iwamoto et al. (1999), and we use their model W7. For single stars, we adopt different sets of stellar yields (see Table 2 and discussion in Sect. 2). Overall, we compute 15 models, which differ only in the adopted nucleosynthesis prescriptions. Another couple of models, Models 1S and 10S, have been computed with different assumptions on the IMF, to let the reader appreciate the IMF effect on the results. They are the same as Models 1 and 10, respectively, but assume a Scalo's (1986) IMF rather than a Kroupa et al.'s (1993) IMF. They are discussed at length in Sect. 6 and are not listed in Table 2. A linear interpolation of the yields is performed as a function of both mass and metallicity. Since none of the massive star studies described in the previous sections includes prescriptions for a 100-M$_{\odot}$ star (see Sect. 2.2), we must extrapolate the yields available for the most massive stellar models. We choose to keep the masses ejected in form of newly produced elements fixed up to 100 M$_{\odot}$.

In the following sections, we present the model predictions and compare them to one another and with the relevant data.

4. Results on the abundance ratios

In this section we discuss, element by element, the behaviour of several abundance ratios as a function of metallicity in the solar neighbourhood, [X/M] versus [M/H]. We show either iron, oxygen or magnesium as the metallicity indicator.

4.1. CNO nuclei

Carbon Carbon is known to form through the 3-α process in stars (Wallerstein et al. 1997, and references therein). However, it is still debated whether it comes mainly from LIMSs or massive stars (see e.g. Henry et al. 2000; Chiappini et al. 2003; Akerman et al. 2004; Carigi et al. 2005; Cescutti et al. 2009, for different points of view).

In Fig. 3, we show the behaviour of [C/O] as a function of [O/H] (panel a) and [C/Fe] as a function of [Fe/H] (panel c) as traced by high-resolution observations of solar neighbourhood stars (symbols). The data are compared to the predictions of selected models (lines).

In order to derive the stellar carbon abundances, spectroscopists rely on high-excitation permitted C I features and on the forbidden [C I] line at 872.7 nm (free from non-LTE effects), as well as on various molecular species, notably CH, C_2 and CO. For solar-type stars, carbon abundances based on the forbidden [C I] line at 872.7 nm are highly accurate, especially if the blending weak feature affecting the line is

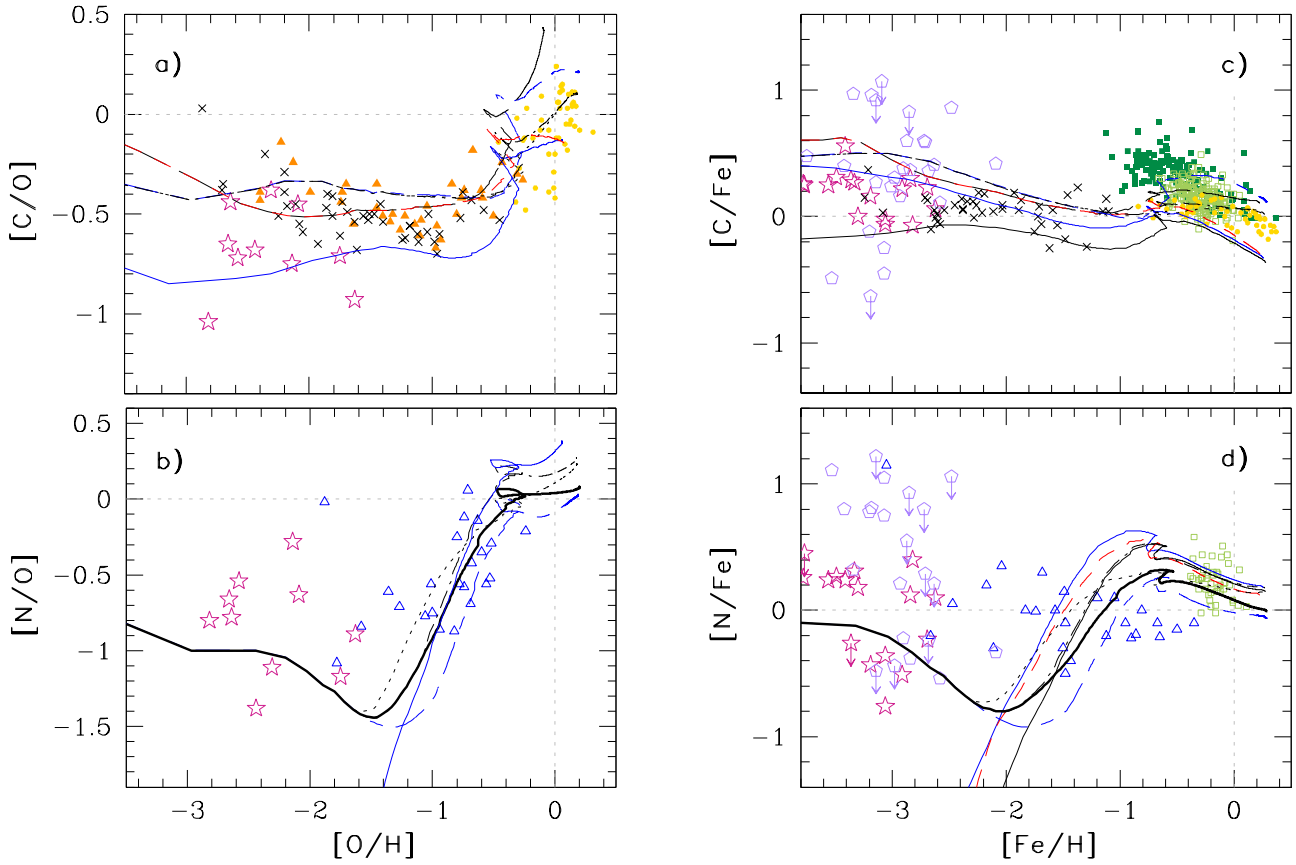

Fig. 3. Left panels: Carbon-to-oxygen (upper panel) and nitrogen-to-oxygen (lower panel) ratios as functions of [O/H] in the solar neighbourhood. Right panels: [C/Fe] (upper panel) and [N/Fe] (lower panel) as functions of [Fe/H] in the solar neighbourhood. Data are from Spite et al. (2005, empty stars), Lai et al. (2008, empty pentagons), Fabbian et al. (2009, crosses), Akerman et al. (2004, filled tringles), Israelian et al. (2004, open triangles), Reddy et al. (2006, filled squares) Reddy et al. (2003, open squares) and Bensby & Feltzing (2006, filled circles). Model predictions are shown for Models 1 [short-dashed (red) lines], 3 [long-dashed (black) lines], 4 [solid (blue) lines], 5 [solid (black) lines], 6 [dot-dashed (black) lines], 9 [dotted (black) lines], 10 [short-dashed-long-dashed (blue) lines] and 15 (thick solid lines). See the electronic edition of the journal for a colour version of this figure.

taken into account (Bensby & Feltzing 2006). According to Bensby & Feltzing (2006), who analyzed the forbidden [C I] line in a sample of 51 nearby F and G dwarf stars, [C/Fe] versus [Fe/H] is flat for subsolar metallicities down to [Fe/H] = −1.0, with no distinctive trends for thin- and thick-disc stars. At higher metallicities, from [Fe/H] ≈ 0 and up to [Fe/H] ≈ +0.4, thin-disc members (which extend to higher metallicities than thick-disc members) show a shallow decline in [C/Fe]. The [C/O] versus [O/H] trends instead are well separated between the two discs, thanks to differences in the oxygen abundances. On the other hand, Reddy et al. (2006), using permitted C I lines, find that the abundance ratios [C/Fe] for the thick disc are on average larger than the [C/Fe] for the thin disc in the metallicity range −1.0 < [Fe/H] < −0.4. Furthermore, [C/Fe] is found to increase with decreasing [Fe/H] at sub-solar metallicities. A trend of increasing [C/Fe] with decreasing [Fe/H] results also from the metal-poor halo stars analyzed by Akerman et al. (2004). In the [C/O] versus [O/H] plot, an upturn in [C/O] is detected towards lower metallicities (Fig. 3, panel a, filled triangles). Akerman et al. (2004) corrected the oxygen abundances for non-LTE effects, but did not apply any non-LTE correction to the [C/O] ratios, under the assumption that non-LTE corrections for the permitted C I and O I lines are of similar size. Recent non-LTE calculations for 43 halo stars by Fabbian et al. (2009) confirm and strengthen the case for an upturn in [C/O] for [O/H] < −2 (Fig. 3, panel a, crosses). The sparse data for extremely metal-poor halo giants by Spite et al. (2005, Fig. 3, stars) should be given a lower weight, because unaccounted 3D effects likely affect the carbon molecular lines employed in the analysis (Asplund 2005).

In the [C/O] versus [O/H] diagram (Fig. 3, panel a), the predictions from Model 1 [short-dashed (red) line], adopting the metallicity-dependent yields of Woosley & Weaver (1995) case B for massive stars, are in satisfactory agreement with the halo data, but fail to reproduce the solar ratio and the trend of increasing [C/O] with increasing [O/H] found for the most metal-rich stars. Maeder's (1992) yields for solar-metallicity stars, computed with high mass loss rates but no rotation, tend to overestimate the [C/O] ratio at high metallicities [Model 3, long-dashed (black) line]. Models 4 and 5, computed using the Kobayashi et al. (2006) yields with $\varepsilon_{\rm HN}$ = 0 and 1, respectively, underestimate the [C/O] ratio in the solar vicinity at all metallicities. Since they predict nearly the same trend, with differences less than 0.2 dex from one another, we show only the results from Model 4 [solid (blue) line]. Models including rotation in high-mass stars (i.e. Model 6 and Models from 8 to 15), slightly overestimate the [C/O] ratio in the Galactic halo, but are, in gen-

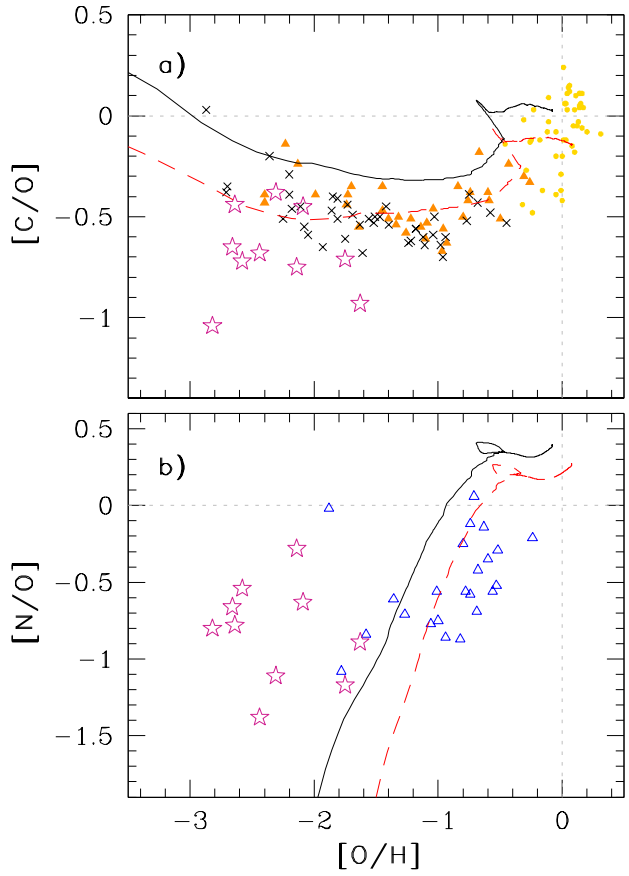

Fig. 4. Carbon-to-oxygen (upper panel) and nitrogen-to-oxygen (lower panel) as functions of [O/H] in the solar neighbourhood. Data (symbols) are the same as in Fig. 3. Also shown are the predictions from Models 1 (short-dashed lines) and 2 (solid lines). The two models differ only in the adopted location of the mass cut in models of SNII explosions. See the electronic edition of the journal for a colour version of this figure.

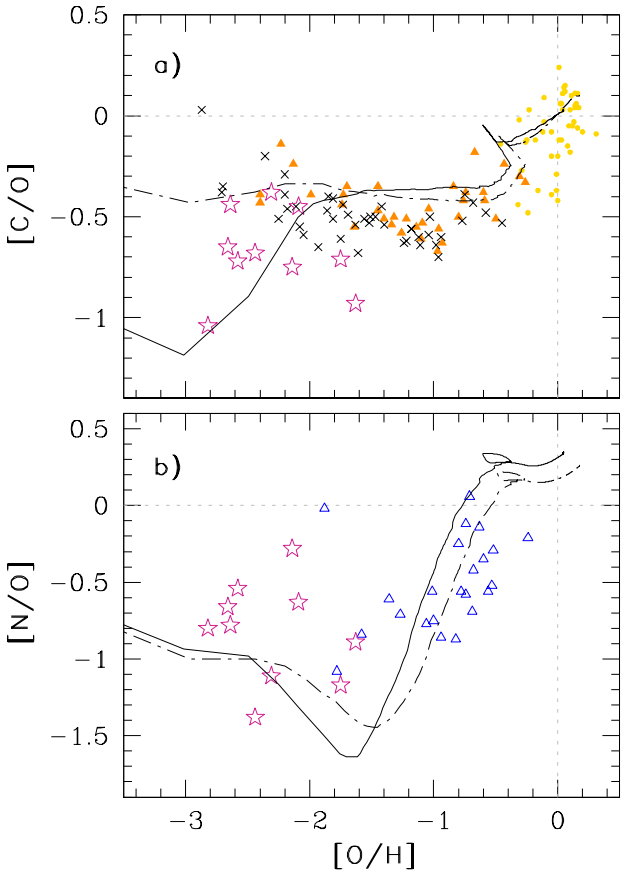

Fig. 5. Same as Fig. 4, but for Models 6 (dot-dashed lines) and 7 (solid lines), adopting the pre-SN yields from the Geneva group with and without rotation, respectively. See the electronic edition of the journal for a colour version of this figure.

eral, in good agreement with the thin-disc and solar data, apart from Models 10–12, that severely overestimate the [C/O] ratios at [O/H] > −0.6. These models use the yields from Marigo (2001) for LIMSs. To avoid overcrowding, in Fig. 3 we show the theoretical predictions only for a subset of models, namely Models 6 [dot-dashed (black) line], 9 [dotted (black) line] and 10 [short-dashed-long-dashed (blue) line].

In the [C/Fe] versus [Fe/H] plot (Fig. 3, panel c), our models predict a decreasing trend of [C/Fe] with increasing metallicity in the metallicity domain −3.0 < [Fe/H] < −1.0. This trend is followed by an increase of [C/Fe] from [Fe/H] = −1.0 to [Fe/H] = −0.5 and, then, by either a shallow decline (Models 1, 4, 5, 10) or a flattening of the ratio (Models 3, 6, 9, 13, 15) towards solar metallicities and up to [Fe/H] = +0.4. Predictions from Models 6, 9, 13 and 15 (the last two not shown in the figure), in particular, are in remarkable agreement with data from Bensby & Feltzing (2006, filled circles in Fig. 3) – free from non-LTE effects – and Fabbian et al. (2009, crosses in Fig. 3) – taking appropriate non-LTE corrections into account. A notable exception is Model 5, computed with Kobayashi et al. (2006) yields for massive stars assuming that 100% of stars with $m \geq 20$ M$_\odot$ explode as HNe [$\varepsilon_{\rm HN} = 1$, lower (black) solid curve in Fig. 3, panel c], which underestimates the [C/Fe] ratio across the whole metallicity range.

All in all, we find differences up to 0.5–0.6 dex in the predicted [C/O] ratios and up to 0.8 dex in the predicted [C/Fe] ratios. This quantifies the uncertainties in the model predictions due to the uncertainties in the adopted stellar yields. The models discussed up to now adopt the best yield sets from different authors, which differ quite a lot in the assumed input physics (see Sect. 2). To evaluate the effect of changing *only one* parameter of stellar evolution on the predictions of GCE models, we run: (i) Model 2, which is the same as Model 1 but for the assumed final kinetic energy of the ejecta from $m \geq 30$ M$_\odot$ stars at infinity (which is lower in Model 2 than in Model 1; see Woosley & Weaver 1995, case A versus case B); (ii) Model 7, which is the same as Model 6 but for the assumed pre-SN yields of He and CNO elements from massive stars (which are now taken from the computations of the Geneva group for *non-rotating* stellar models); (iii) Model 8, which differs from Model 6 only in the assumed parameter of mass loss along the AGB (which is constant with metallicity rather than varying with Z in Model 8) and from Model 9 in that HBB is allowed to operate in a smaller mass range in Model 9; (iv) Model 11, which is the same as Model 10 but for the assumed mixing-length parameter for intermediate-mass stars ($\alpha = 2.50$ rather than 1.68 – this parameter mainly affects the production of ^{4}He and ^{14}N due to HBB; Marigo 2001).

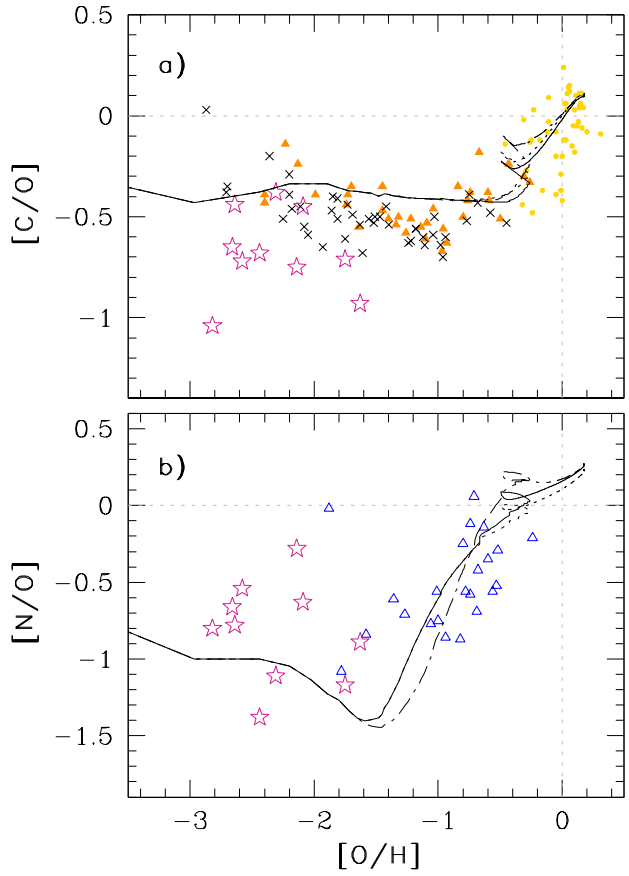

Fig. 6. Same as Fig. 4, but for Models 6 (dot-dashed lines), 8 (solid lines) and 9 (dotted lines). Models 6 and 8 differ only in the adopted parameter of mass loss along the AGB, Models 8 and 9 in the assumed mass range in which HBB can take place. See the electronic edition of the journal for a colour version of this figure.

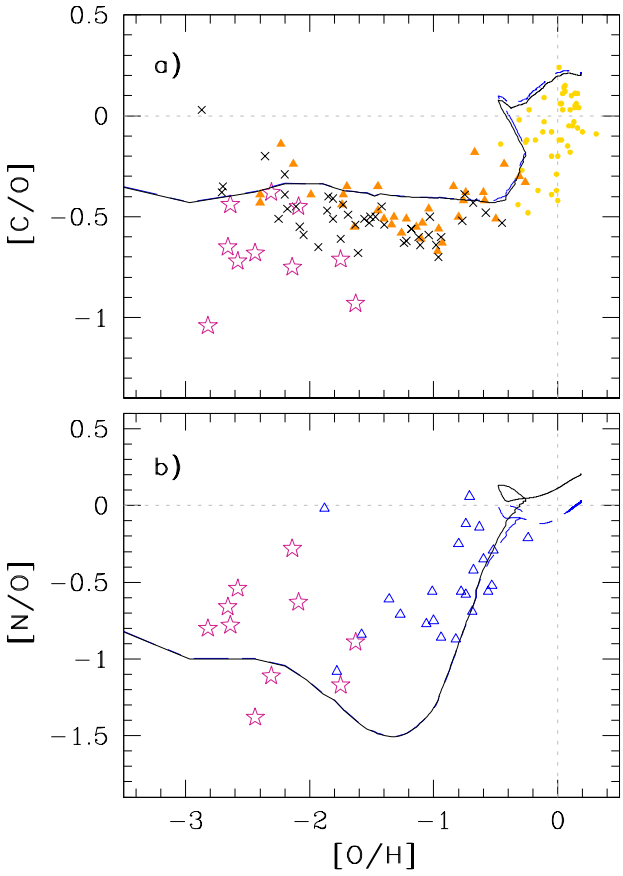

Fig. 7. Same as Fig. 4, but for Models 10 (short-dashed-long-dashed lines) and 11 (solid lines), which differ only in the assumed mixing-length parameter for intermediate-mass star models. See the electronic edition of the journal for a colour version of this figure.

The predictions of Model 2 versus Model 1, Model 7 versus Model 6, Model 8 versus Models 6 and 9, and Model 11 versus Model 10 regarding the behaviour of [C/O] versus [O/H] in the solar neighbourhood are shown in the top panels of Figs. 4, 5, 6 and 7, respectively. It is seen that changing the mass cut in models of SNII explosions has a profound impact on the predicted [C/O] at all metallicities. The inclusion of rotation in models of high-mass stars substantially changes the predictions on the [C/O] ratio for [O/H] < -2. Smaller (or even negligible) effects are seen at higher metallicity in dependence on the assumed mass loss and/or HBB efficiency in LIMSs.

Nitrogen Nitrogen is synthesized through the CNO cycle in the star hydrogen-burning layers (Clayton 1983; Arnett 1996). It was recognized long ago that LIMSs are net producers of (primary and secondary) nitrogen on a Galactic scale (Edmunds & Pagel 1978; Renzini & Voli 1981). While it was suggested years ago that metal-poor massive stars needed to significantly contribute to the production of primary nitrogen (see e.g., Matteucci 1986), only recently has the physical mechanism been identified as rotation (Meynet & Maeder 2002b).

In the [N/Fe] versus [Fe/H] diagram, the interpretation of the observations and the search for any abundance trends are complicated by the fact that the stellar abundances show considerable scatter at a fixed [Fe/H], which is largely attributable to the weakness of the usable spectral lines and/or to the $T_{\rm eff}$ sensitivity of the derived abundances. Indeed, in late-type stars one can rely only on weak, high-excitation near-IR N I lines, also subject to non-LTE line formation and 3D effects. In halo stars, only the NH and CN molecular lines can be observed, and both have disadvantages. The NH band-head falls in a crowded region of the spectra, whereas an analysis of the CN lines requires a priori knowledge of carbon abundances. Furthermore, both lines are affected by 3D effects, that for NH can result in -0.6 and -0.9 abundance corrections for turn-off stars at [Fe/H] $= -2$ and [Fe/H] $= -3$, respectively, with giants having not been investigated yet (Asplund 2005, and references therein).

The [N/O] versus [O/H] plot is another powerful diagnostic diagram, but once again literature data need corrections owing to non-LTE and 3D effects. Israelian et al. (2004) estimated robust [N/O] ratios for 31 unevolved metal-poor stars using nitrogen and oxygen abundances from near-UV NH and OH lines. Although their [N/O] (Fig. 3, panel b, empty triangles) should stay basically intact, the [O/H] values would decrease by ~ 0.5 dex in 3D (Asplund 2005). More severe corrections should affect the [N/O] ratios derived by Spite et al. (2005, Fig. 3, panel b, stars): Asplund (2005) estimates that they would decrease by ~ 0.4 dex, while lower negative corrections of ~ 0.2 dex should

apply to the [O/H] values. This would lead to a slowly increasing trend of [N/O] with [O/H] even at the lowest metallicities.

Being aware of all the shortcomings affecting both the data and the models, we show the predictions of some of our models for [N/O] versus [O/H] and [N/Fe] versus [Fe/H] in Fig. 3, panels b and d, respectively. Other predictions from models where the parameters of stellar evolution are changed one at a time, are shown in Figs. 4 to 7 (only for [N/O] versus [O/H]). Model predictions are compared to data from Spite et al. (2005), Lai et al. (2008), Israelian et al. (2004), and Reddy et al. (2003). It is apparent that only Models 6 to 15, adopting the N yields from low-metallicity massive stars from the Geneva group, are able to explain the current measurements of [N/O] and [N/Fe] in very metal-poor halo stars (see also Ekström et al. 2008, their figure 9). The most massive zero-metallicity stars produce great amounts of N independently of the assumed stellar rotation (see Ekström et al. 2008, their table 4). As a consequence, a plateau in [N/O], [N/O] ~ -0.9, is found for [O/H] < -2.5 when assuming the Geneva group yields (Fig. 5, lower panel), independently of whether zero-metallicity stars rotate fast or do not rotate at all. However, all the models severely underestimate the [N/O] ([N/Fe]) ratio in the metallicity range $-2 <$ [O/H] < -1 ($-3 <$ [Fe/H] < -1). A contribution to the N enrichment from the winds of super-AGB stars could improve the model predictions. On the other hand, in the framework of our models, a range in [Fe/H] from -3 to -1 corresponds to a range in overall metallicity Z from about 4×10^{-5} to about 0.002. In this metallicity range, we are using the yields obtained by interpolating the grids computed by Meynet & Maeder (2002a) for massive slow rotators with $Z = 10^{-5}$ and $Z = 0.004$. Thus, the predicted deficiency of nitrogen could unravel the need for an upward revision of Meynet & Maeder's (2002a) N yields. This could be achieved by making the stars rotate faster at those metallicities (the faster the stellar rotation, the larger the primary N production; Meynet & Maeder 2002b).

Changing the prescriptions about N production in LIMSs has a profound impact on the theoretical predictions at higher metallicities, [O/H] > -1.4 and [Fe/H] > -2.0. It is clear that both changing the rate of mass loss along the AGB and the efficiency of HBB in models of intermediate-mass stars play a significant role in shaping the model predictions for N (see the lower panels of Figs. 6 and 7, respectively). Differences up to 0.7 dex in both [N/O] and [N/Fe] are found at intermediate metallicities for models keeping the same nucleosynthesis prescriptions for massive stars and changing those for LIMSs (cfr. predictions from Models 9 and 10, dotted and short-dashed-long-dashed lines, respectively, in Fig. 3, panels b and d). Model 15, which assumes the revised N yields by Karakas (2010) for LIMSs, is the only one which fits best both the solar [N/O] and [N/Fe] ratios (Fig. 3, thick solid line).

Oxygen Next to hydrogen and helium, oxygen is the third most abundant element in the universe. It forms essentially in the interiors of massive stars, through hydrostatic burning of He, C, and Ne (e.g. Arnett 1996). Available indicators of oxygen abundances in stars include the O I triplet at ~7774 Å (mainly observed in FG dwarfs and subgiants), the forbidden [O I] lines at 6300 and 6363 Å (detected in giants and cool subgiants, and barely detectable in dwarfs), and the OH lines in the UV (observed in FGK metal-poor stars) and in the IR (only observed in cool stars with $T_{\rm eff} < 5000$ K). The features at 7774 Å are strong and located in a clean part of the spectrum but subject to large and poorly understood deviations from LTE conditions.

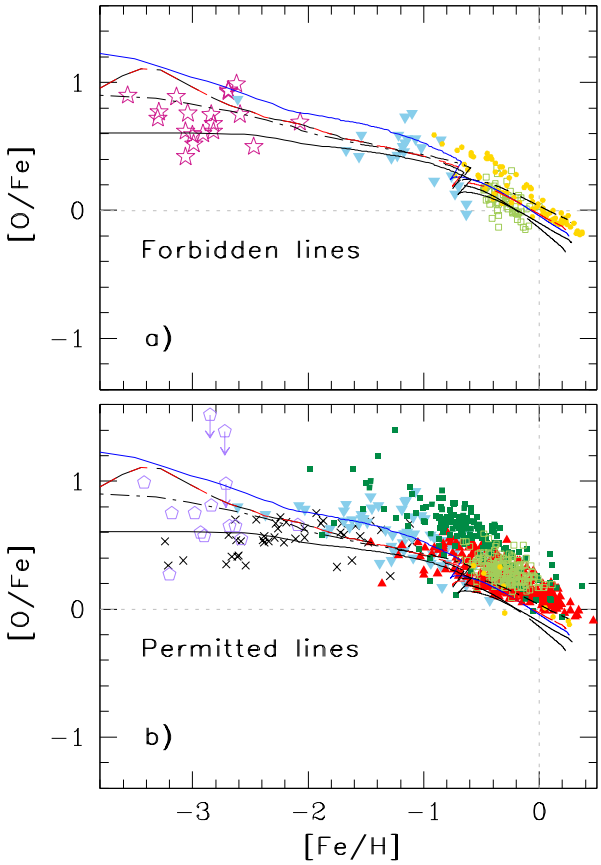

Fig. 8. [O/Fe] versus [Fe/H] in the solar neighbourhood. Theoretical predictions are from Models 1 [short-dashed (red) lines], 3 [long-dashed (black) lines], 4 [upper (blue) solid lines], 5 [lower (black) solid lines] and 6 [dot-dashed (black) lines]. Upper panel: oxygen abundances from the forbidden [O I] lines from Cayrel et al. (2004, stars), Gratton et al. (2003, upside-down triangles), Reddy et al. (2003, open squares) and Bensby et al. (2005, filled circles). Lower panel: oxygen abundances from other indicators from Lai et al. (2008, open pentagons), Fabbian et al. (2009, crosses), Gratton et al. (2003, upside-down triangles), Reddy et al. (2006, filled squares), Reddy et al. (2003, open squares), Ramírez et al. (2007, triangles) and Bensby et al. (2005, filled circles). See the electronic edition of the journal for a colour version of this figure.

The forbidden lines are free from non-LTE effects but weak and blended by lines from other chemical species. Furthermore, switching from 1D to 3D models changes the [O I]-based abundances by as much as -0.2 dex in turn-off stars with [Fe/H] $= -2$; a similar behaviour can be anticipated for metal-poor giants (Nissen et al. 2002). The OH lines are difficult to observe and, in the UV domain, are also affected by surface inhomogeneities. The most reliable indicators of oxygen abundances in stars seem to be the forbidden [O I] lines (see volume 45 issue 8 of New Astronomy), especially if spectra of high resolution and high S/N are acquired and analyzed using accurate atomic line data (Nissen et al. 2002).

In Fig. 8 we compare some of our oxygen model predictions to observations of the forbidden [O I] line as well as of other oxygen lines (panels a and b, respectively), concentrating on models which adopt the best yield sets suggested by different authors.

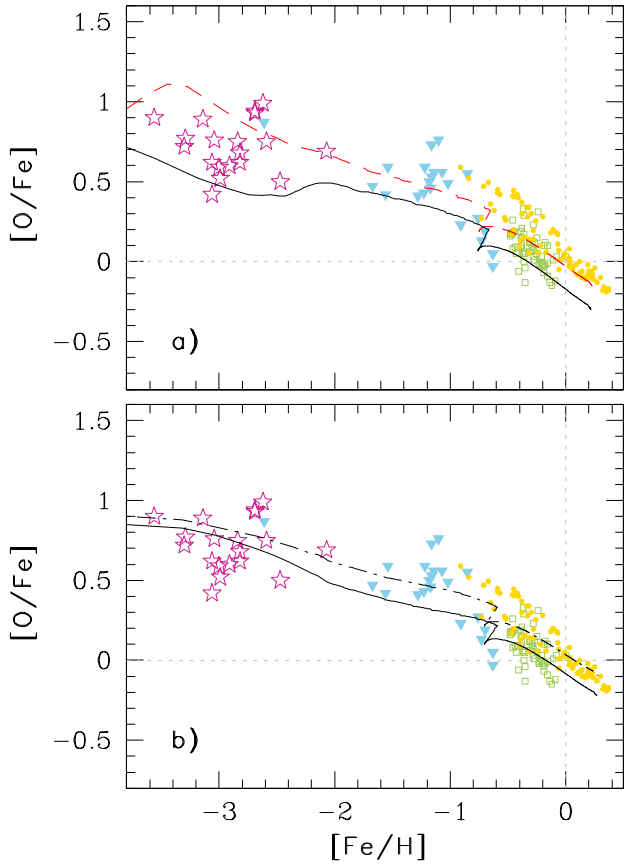

Fig. 9. Upper panel: predictions on [O/Fe] versus [Fe/H] from Models 1 and 2 [short-dashed (red) and solid (black) lines, respectively] are compared one to another and with data from the forbidden [O I] lines (see Fig. 8 caption for references). Lower panel: same as the upper panel, but for Models 6 and 7 [dot-dashed and solid (black) lines, respectively]. See the electronic edition of the journal for a colour version of this figure.

Models 1, 6, 8, 9, 10, 11, 13 and 15[3] forecast an [O/Fe] ratio which, starting from [O/Fe] $\simeq +1$ at [Fe/H] $\simeq -4$, slopes gently down to subsolar values at the highest metallicities. This is in excellent agreement with the observations, especially if the [O I]-based abundances are considered for comparison. The gradual increase of [O/Fe] with decreasing [Fe/H] in the [Fe/H] < -1 regime stems from the larger oxygen-to-iron ratios in the ejecta of more massive, more metal-poor SNeII. The quick decrease of [O/Fe] above [Fe/H] $\simeq -1$ is due instead to the overwhelming contribution to the Fe production by SNeIa. Models 3, 12 and 14, assuming Maeder's (1992) yields for solar-metallicity massive stars, predict a decrease of the [O/Fe] ratio at high metallicities definitely steeper than indicated by trustworthy data from Bensby et al. (2005, Fig. 8, panel a, filled circles). In order to avoid overcrowding, only the predictions from Model 3 are shown [Fig. 8, long-dashed (black) curves]. Model 4, adopting the yields by Kobayashi et al. (2006) for normal SNe, fits the disc and Sun data nicely [Fig. 8, upper (blue) solid curve]. However, it slightly overestimates the halo data. Model 5, instead, assuming that all stars above 20 $M_\odot$ explode as HNe with much higher explosion energies, predicts an almost flat [O/Fe] versus [Fe/H] trend in the early halo [Fig. 8, lower (black) solid line]. Though most of the observed [O/Fe] ratios lie above the theoretical predictions, there are some stars whose abundances are consistent with a scenario of formation from pure HN ejecta.

It is common belief that the synthesis of O in stars is well understood. Yet, by using different prescriptions on the O production in stars, we find that the predicted [O/Fe] ratio may vary by as much as 0.6 dex at the lowest metallicities. The difference reduces to 0.2 dex at solar metallicity. At the origin of the uncertainties in the predictions of our GCE model there is, once again, the complex interplay among the different assumptions made by different authors working on stellar evolution and nucleosynthesis to treat the different processes regulating the evolution of the stars. In Fig. 9, upper panel, we compare the predictions of Models 1 and 2, which differ only in the location of the mass cut in models of SNII explosions. It is seen that a variation in this parameter may have a huge impact (up to 0.5 dex) on the predicted [O/Fe] at the lowest metallicities. Stellar rotation has a lower – still non-negligible – impact (see Fig. 9, lower panel).

4.2. Odd-Z elements

Sodium Sodium is an odd-Z element, synthesized mostly during hydrostatic carbon burning, and partly during hydrogen burning through the NeNa cycle; the *s*-process produces some Na as well (Clayton 2003). Adopting the LTE approximation in standard abundance analyses of Na can lead to substantial overestimates of the Na abundances. Non-LTE abundance corrections can be very large, typically −0.1 dex at solar metallicity and −0.5 dex or more at [Fe/H] around −2, for the 589 and 819 nm doublets; the departures from LTE become less severe for [Fe/H] < -2 as the line formation shifts to deeper layers (e.g. Baumüller et al. 1998). The weaker 568 and 615 nm doublets are less sensitive to non-LTE effects. Departures from LTE are most likely the culprits for the discordant values of [Na/Fe] reported in the literature for metal-poor stars (see Reddy et al. 2006, and references therein). From their LTE analysis of the Na I lines at 6154 and 6160 Å, Reddy et al. (2006) find a hint for an increase of [Na/Fe] with increasing [Fe/H] in the metallicity range $-1.0 <$ [Fe/H] < -0.6, followed by a decrease towards solar values for $-0.6 <$ [Fe/H] < 0. Such a trend is confirmed by Shi et al. (2004) using non-LTE statistical equilibrium calculations. For [Fe/H] > 0, Bensby et al. (2003, 2005) observe a rise in the [Na/Fe] trend, which was also seen by Edvardsson et al. (1993). As for the lowest metallicities, when only extremely metal-poor dwarfs and unmixed giants are considered and the non-LTE corrections of the Na abundances are taken into account, one gets a flat trend of the [Na/Fe] ratio in the metallicity regime $-4.0 <$ [Fe/H] < -2.5, $[\mathrm{Na/Fe}]_{\mathrm{NLTE}} = -0.21 \pm 0.13$ dex, and a small star-to-star variation, comparable to that found for other elements (Andrievsky et al. 2007).

As one can see in Fig. 10, panel a, only Model 4 [upper solid (blue) curve], corresponding to the yields by Kobayashi et al. (2006) for massive stars without HNe, predicts a [Na/Fe] ratio in agreement with the halo data. Models including nucleosynthesis from HNe, namely, Models from 5 to 15 [for sake of clarity, only the predictions from Model 5 are shown in the figure, lower solid (black) curve], underestimate the [Na/Fe] ratio in the halo. Model 1 [short-dashed (red) line], adopting the yields of Woosley & Weaver (1995) case B, provides an acceptable fit to the halo ratios, but only in the $-2.5 \leq$ [Fe/H] ≤ -1 metallicity range. All in all, at the lowest metallicities we find differences up

[3] For sake of clarity, only the predictions from Models 1 and 6 are shown in Fig. 8 [short-dashed (red) and dot-dashed (black) lines, respectively].

to 1.4 dex in the predicted [Na/Fe] ratio which, similarly to what we found for the [O/Fe] ratio, are largely driven by the adopted mass cut and energy of the explosion in models of massive stars. These differences reduce to ~0.2 dex at [Fe/H] > −2.

Models from 1 to 12 do not account for Na synthesis from LIMSs. If Na production from LIMSs is considered, very different predictions for Na evolution in the disc are found, depending on the adopted yields. Model 15, adopting the revised Karakas (2010) yields of Na from LIMSs (Fig. 11, panel a, thick solid line) predicts an almost negligible production of sodium from these stellar sources on a Galactic scale. The adoption of the old Karakas & Lattanzio (2007) yields, instead, leads to a huge Na production from LIMSs in the disc (Fig. 11, panel a, thick dotted line). These differences in model predictions for Na are essentially due to the up-to-date nuclear reaction rates adopted by Karakas (2010, see discussion in Sect. 2). None of the models, however, is able to explain the intriguing upward trend of [Na/Fe] at [Fe/H] > 0, first pointed out by Edvardsson et al. (1993) and clearly seen in the Bensby et al. (2005) data (filled circles in Fig. 11). None of the models includes Na production from rotating massive stars. We will come back to this point in Sect. 7.

Aluminium Aluminium is a product of hydrostatic carbon and neon burning (e.g. Woosley & Weaver 1995). It can also be produced during hydrogen burning in the MgAl chain. Observationally, Al abundances need large non-LTE corrections: at solar [Fe/H], they amount to approximately +0.1 dex for the Al I 396 nm resonance line, but reach +0.4 dex or even more for [Fe/H] < −1.0; the maximum correction, +0.8 dex, is required for mildly metal-poor turn-off stars in which the line is saturated (Asplund 2005). For [Fe/H] > −1.0, Al shows a 'Mg-like behaviour' (Bensby et al. 2003, 2005; Reddy et al. 2006). At very low metallicities, [Fe/H] < −2.8, the relation [Al/Fe] versus [Fe/H] becomes rather flat, $[Al/Fe]_{NLTE} = -0.06 \pm 0.10$ (Andrievsky et al. 2008); the scatter around the mean value is smaller than the scatter of the LTE determinations (Cayrel et al. 2004) and can be explained by measurement errors only. A few sparse data are available in the intermediate metallicity regime. Here, the non-LTE [Al/Mg] ratio displays an intriguing step-like difference between stars belonging to the Galactic halo and disc populations, that might prove useful as a further membership diagnostic criterion (see Gehren et al. 2006, and discussion therein). We will come back to this issue later.

In the low-metallicity domain, the best-fitting models are those adopting Kobayashi et al. (2006) yields for massive stars with $\varepsilon_{HN} = 1$ (see Table 2; only predictions from Model 5 are shown in Fig. 10). Such models predict an almost constant [Al/Fe] ratio during the first 370 Myr of Galactic evolution. Then, the ratio increases mildly, owing to the metal dependency of Al production in massive stars, and flattens again around a Galactic age of 1 Gyr, because of the increasing Fe production from SNeIa. None of the models can explain the behaviour of [Al/Fe] in the Galactic disc. The activation of the MgAl chain in the central regions of rotating massive stars on the main sequence, followed by transportation of Al-rich matter to the outer envelope and ejection of the outermost layers by slow stellar winds, might lead to a substantial modification of the Al yields used here (Decressin et al. 2007). However, complete grids of Al yields from rotating massive stars are not available yet. Also, one must be aware that, in order to reproduce the Mg-Al anticorrelation observed in globular clusters stars, Decressin et al. (2007) varied the rate of the nuclear reaction $^{24}Mg(p, \gamma)^{25}Al$ by orders of magnitude outside of the published uncertainties.

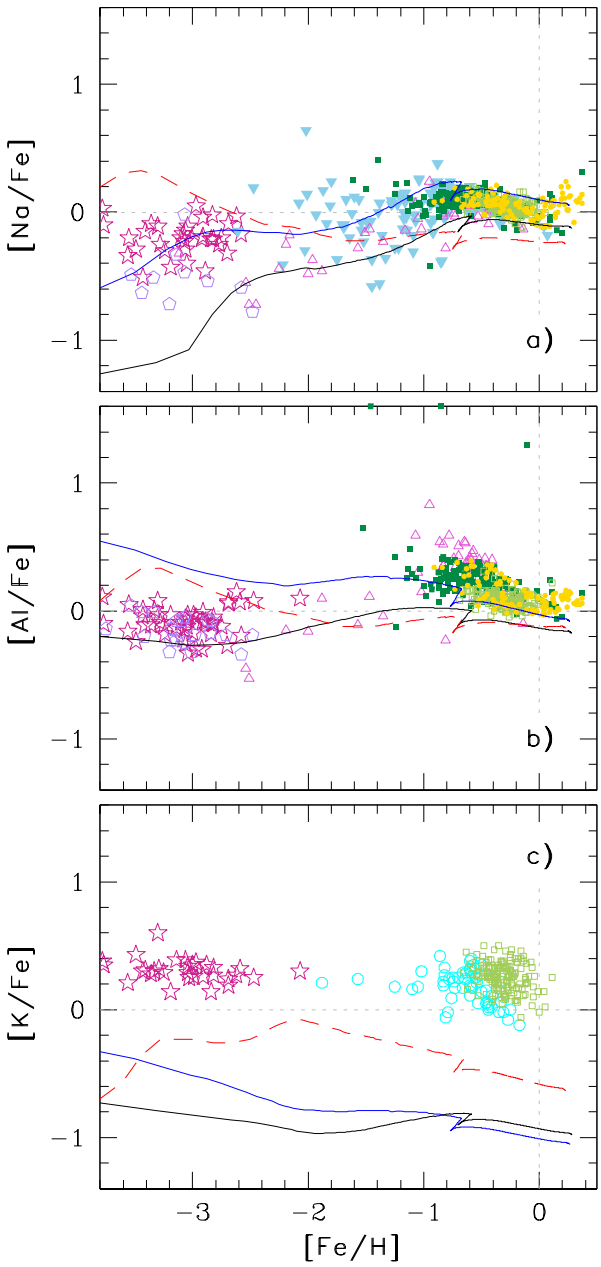

Fig. 10. [X/Fe] versus [Fe/H] relations for sodium (panel a), aluminium (panel b) and potassium (panel c) in the solar neighbourhood. Theoretical predictions are from Models 1 [short-dashed (red) lines], 4 [upper solid (blue) lines] and 5 [lower solid (black) lines]. Data are from Andrievsky et al. (2007, 2008, 2010, stars, for Na, Al and K, respectively), Lai et al. (2008, open pentagons), Gratton et al. (2003, upside-down triangles), Gehren et al. (2006, open triangles), Zhang et al. (2006, open circles), Reddy et al. (2006, filled squares), Reddy et al. (2003, open squares) and Bensby et al. (2005, filled circles). LTE abundances from Lai et al. (2008) have been corrected by −0.5 dex for Na (Baumüller et al. 1998) and +0.65 dex for Al (Baumüller & Gehren 1997). See the electronic edition of the journal for a colour version of this figure.

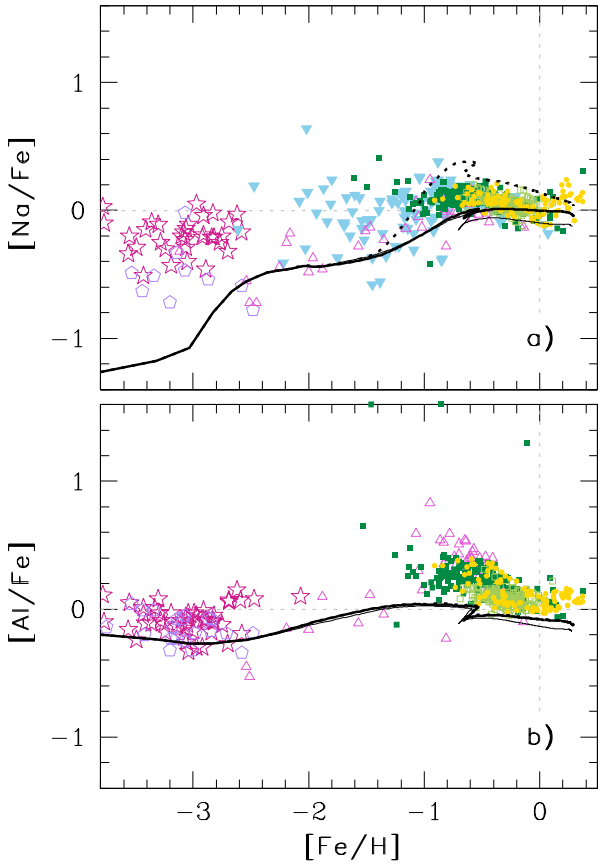

Fig. 11. Same as Fig. 10, panels a and b, but for Models 5 (thin solid lines), 13 (thick dotted lines) and 15 (thick solid lines). The predictions for [Al/Fe] versus [Fe/H] from Model 15 lay on those from Model 13. See the electronic edition of the journal for a colour version of this figure.

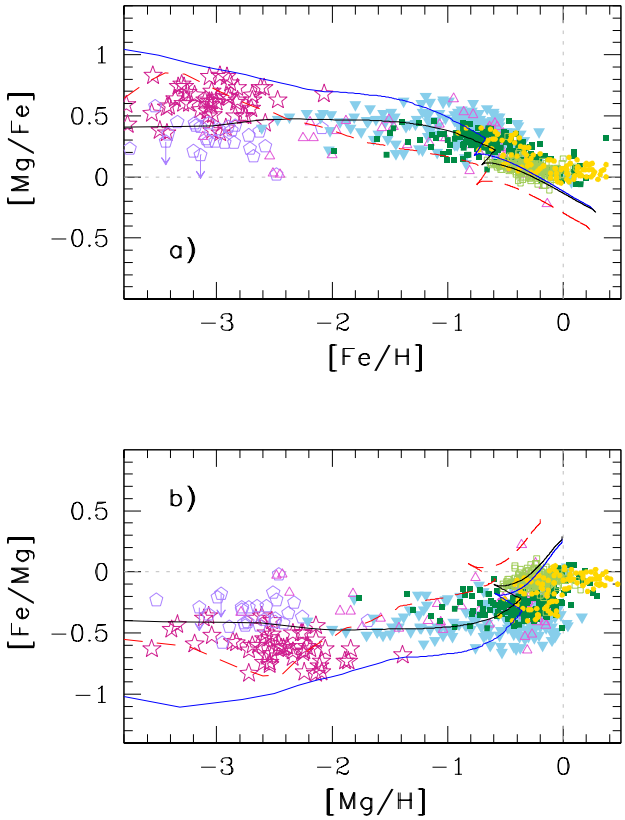

Fig. 12. [Mg/Fe] versus [Fe/H] (top panel) and [Fe/Mg] versus [Mg/H] (bottom panel) in the solar neighbourhood. Theoretical predictions are from Models 1 [short-dashed (red) lines], 4 [upper solid (blue) line in panel a and lower solid (blue) line in panel b] and 5 [lower solid (black) line in panel a and upper solid (black) line in panel b]. Data are from Andrievsky et al. (2010, stars), Lai et al. (2008, open pentagons), Gratton et al. (2003, upside-down triangles), Gehren et al. (2006, open triangles), Reddy et al. (2006, filled squares), Reddy et al. (2003, open squares) and Bensby et al. (2005, filled circles). See the electronic edition of the journal for a colour version of this figure.

The role of Al production from LIMSs should be better investigated as well: the recent study by Karakas (2010) ascribes almost no Al production to LIMSs (Fig. 11, lower panel, thick solid line), confirming results from previous work by Karakas & Lattanzio (2007, Fig. 11, lower panel, thick dotted line). If AGB stars are responsible for the globular cluster Mg-Al anticorrelation, then it is likely that AGB stars as a whole synthesize more Al than predicted by current models (Marcolini et al. 2009). Should a significant amount of Al come from LIMSs, a sudden rise of the [Al/Fe] ratio in field Galactic stars would be obtained starting at [Fe/H] ~ -1.5 (cfr. Fig. 11, panel a, thick dotted line, showing the results of Model 13, with a great Na production from LIMSs), in agreement with the trend inferred from the observations.

Although the uncertainties in the GCE model predictions for Al are by far less dramatic than those for Na, especially in the high metallicity domain, the comparison with the available Al abundance data clearly shows that the synthesis of Al at disc metallicities is still far from having been understood.

Potassium The alkali element potassium is mostly produced by a combination of hydrostatic oxygen shell burning and explosive oxygen burning in proportions that vary depending on the stellar mass (e.g. Woosley & Weaver 1995, and references therein). LTE abundances obtained from the K I 769.9 nm resonance line are overestimated by 0.4–0.7 dex over a wide range of metallicities; non-LTE corrections are smaller, but remain significant (from −0.15 dex to −0.3 dex), for the $\lambda\lambda$ 12522, 12432, and 11769 Å weak subordinate lines (Ivanova & Shimanskiĭ 2000).

In Fig. 10, panel c, we compare our potassium model predictions to the data by Andrievsky et al. (2010), Zhang et al. (2006) and Reddy et al. (2003). Non-LTE corrections are taken into account in the first two studies. Variations up to 1 dex in [K/Fe] are found among different model predictions. The comparison between data and model predictions shows the absolute inadequacy of the adopted stellar yields.

4.3. Alpha elements

Magnesium Most of magnesium comes from hydrostatic carbon burning and explosive neon burning in massive stars (e.g. Woosley & Weaver 1995). Stellar spectroscopists may rely on several Mg I lines, as well as on a few Mg II lines, to derive

magnesium abundances. Non-LTE corrections are of little concern in this case; they are negative for the high-excitation Mg II lines and the Mg I b triplet at 517 nm (−0.05 dex and −0.2 dex at most at low [Fe/H], respectively), while they are positive for the remaining lines, the maximum correction being +0.2 dex at low [Fe/H] (Asplund 2005, and references therein; but see Andrievsky et al. 2010, pointing to somehow larger corrections).

GCE models adopting the yields of Mg by Woosley & Weaver (1995) for massive stars underestimate the abundance of magnesium in the discs of the Galaxy (see Fig. 12, short-dashed lines, referring to case B; see also Timmes et al. 1995; Goswami & Prantzos 2000), unless ad hoc adjustments are made to the yields (François et al. 2004). While detailed nucleosynthesis calculations still have to establish whether the modifications proposed by François et al. (2004) have a physical ground, HNe can provide an alternate solution:

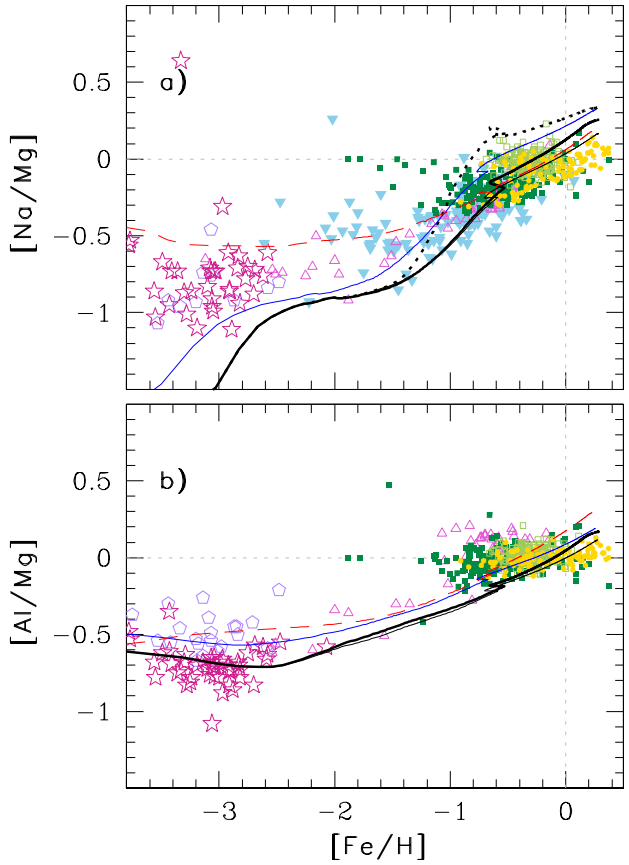

Fig. 13. [X/Mg] versus [Fe/H] relations for sodium (panel a) and aluminium (panel b) in the solar neighbourhood. Theoretical predictions are from Models 1 [short-dashed (red) lines], 4 [upper solid (blue) lines], 5 [lower solid (black) lines], 13 (thick dotted line) and 15 (thick solid lines). Data are from Andrievsky et al. (2007, 2008, 2010, stars, for Na, Al and Mg abundances, respectively), Lai et al. (2008, open pentagons), Gratton et al. (2003, upside-down triangles), Gehren et al. (2006, open triangles), Reddy et al. (2006, filled squares), Reddy et al. (2003, open squares) and Bensby et al. (2005, filled circles). LTE abundances from Lai et al. (2008) have been corrected by −0.5 dex for Na (Baumüller et al. 1998) and +0.65 dex for Al (Baumüller & Gehren 1997). See the electronic edition of the journal for a colour version of this figure.

Kobayashi et al. (2006) have obtained a nice fit to the [Mg/Fe] versus [Fe/H] relation traced by solar neighbourhood stars using a GCE model for the solar vicinity which adopts their new nucleosynthetic yields for SNeII and HNe, $\varepsilon_{\rm HN} = 0.5$ for the HN fraction and a Salpeter IMF. Yet, their model can not reproduce values of [Mg/H] exceeding solar, at odds with observations (see Kobayashi et al. 2006, their figure 9). Here we reasses the problem of Mg evolution, adopting a different GCE model, with a steeper IMF (Kroupa et al. 1993), better suited to describe the stellar populations of the Milky Way field (see Paper I, and references therein), and slightly different mass limits for the IMF, $m_l = 0.1$ M$_\odot$ and $m_u = 100$ M$_\odot$, rather than $m_l = 0.07$ M$_\odot$ and $m_u = 50$ M$_\odot$ as in Kobayashi et al. (2006). If we trust the non-LTE Mg abundances recently computed by Andrievsky et al. (2010) for the most metal-poor stars, the best fit to the observed [Mg/Fe] versus [Fe/H] and [Fe/Mg] versus [Mg/H] relations is obtained with Kobayashi et al. (2006) yields and $\varepsilon_{\rm HN}$ values intermediate between the two extreme cases analysed here (solid lines in Fig. 12). On the other hand, if the LTE Mg abundances by Lai et al. (2008) are the ones to be trusted, the extreme case of $\varepsilon_{\rm HN} = 1$ is favoured instead. None of the models, however, is able to reproduce the highest [Mg/H] values and the flattening of the relations at nearly solar/higher than solar metallicities. This could suggest the need for either a revision of current SNII and/or HN yields for solar and/or higher than solar metallicity stars, or larger contributions to Mg production from SNeIa, or significant Mg synthesis in LIMSs, or a combination of all these factors. Clearly, it is not safe to use Mg as the prime metallicity indicator in metal-rich galaxies.

It has been recently pointed out by Gehren et al. (2006) that, while the trend of [Na/Mg] versus [Fe/H] is witnessing a history of continuous enrichment from the halo to the discs, the [Al/Mg] ratio displays a much more interesting step-like behaviour, with halo stars sharing a common value of $\langle$[Al/Mg]$\rangle \sim -0.45$ and the two disc populations mostly consistent with $\langle$[Al/Mg]$\rangle \sim +0.10$. At the lowest metallicities, say $-3.6 <$ [Fe/H] < -2.5, extremely metal-poor stars share a lower value, $\langle$[Al/Mg]$\rangle \sim -0.7$ (Andrievsky et al. 2010). In Fig. 13 we show these data, together with measurements from other authors. Superimposed are our theoretical tracks, for a significant subset of models (lines). Three results are immediately apparent from this figure. The first is that all models overpredict the [Na/Mg] and [Al/Mg] ratios at [Fe/H] > 0, thus reinforcing the demand for a Mg production higher than predicted by current GCE models at late times. The second important result is that the step-like behaviour of [Al/Mg] versus [Fe/He], suggested by Gehren et al. (2006), can not be reproduced by the models. A jump in [Al/Mg] at [Fe/H] ≈ -1 could be achieved if LIMSs were efficient Al producers (cfr. Model 13 predictions for Na – thick dotted line in Fig. 13, panel a). Finally, it is seen that different models predict almost the same [Al/Mg] versus [Fe/H] behaviour in the solar neighbourhood (Fig. 13, bottom panel), whereas the theoretical [Na/Mg] versus [Fe/H] relations may differ by as much as 0.5–1.0 dex or even more at the lowest metallicities (Fig. 13, top panel). The best description of the observational [Na/Mg] versus [Fe/H] diagram would be obtained with a model assuming a set of yields for massive stars intermediate between the two sets used in Models 1 and 5, namely, Woosley & Weaver (1995) case B and Kobayashi et al. (2006) with $\varepsilon_{\rm HN} = 1$, respectively (see Table 2).

Silicon Silicon is produced mostly during oxygen burning and its final abundance in the stellar ejecta is sensitive to a variety of

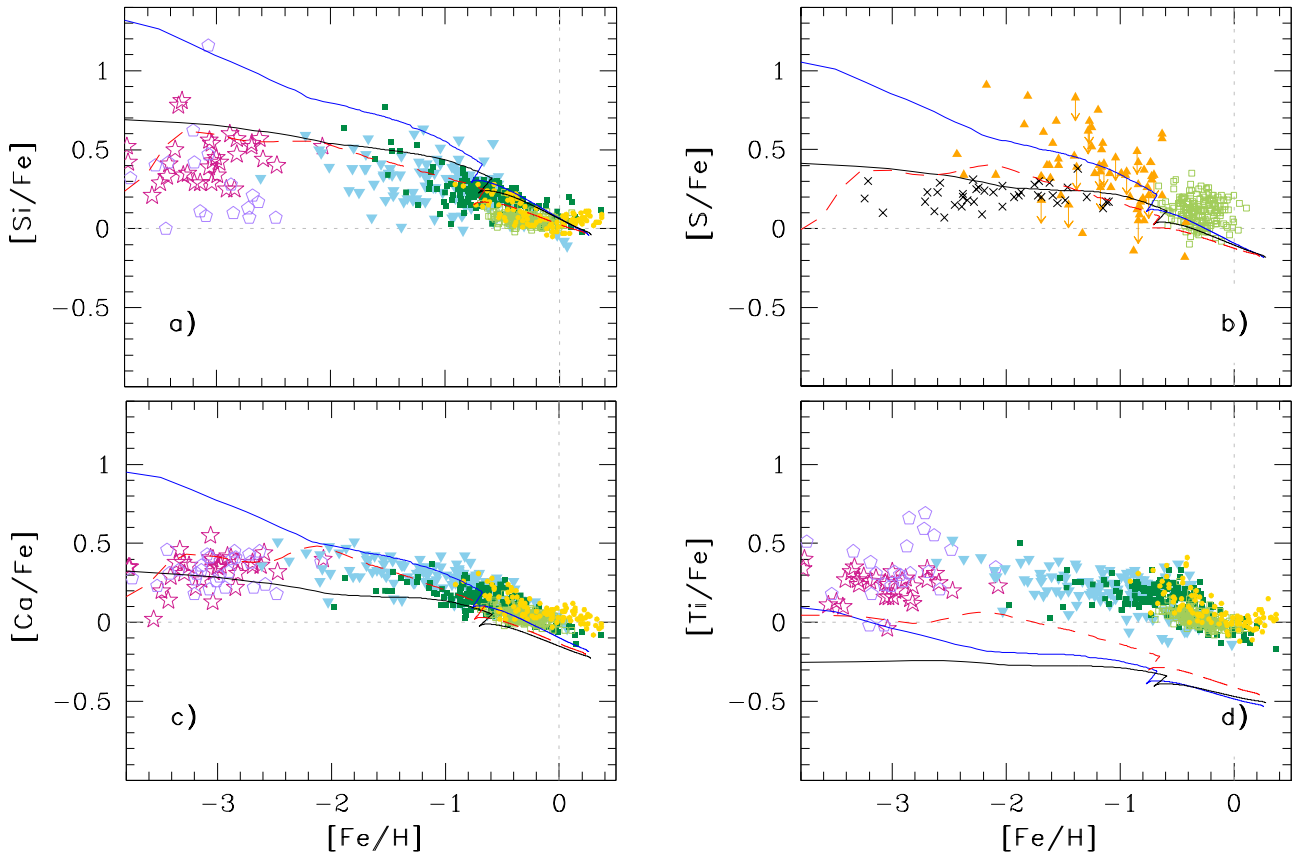

Fig. 14. Predicted behaviour of the relative ratios of several α elements to iron (panel a: silicon, panel b: sulphur, panel c: calcium, panel d: titanium) with respect to the relative iron abundance in the solar neighborhood, for Models 1 [short-dashed (red) lines], 4 [upper solid (blue) lines] and 5 [lower solid (black) lines]. Also shown are data from Cayrel et al. (2004, stars), Lai et al. (2008, open pentagons), Nissen et al. (2007, crosses), Gratton et al. (2003, upside-down triangles), Caffau et al. (2005, triangles), Reddy et al. (2006, filled squares), Reddy et al. (2003, open squares) and Bensby et al. (2005, filled circles). See the electronic edition of the journal for a colour version of this figure.

factors regulating the evolution and explosion of the progenitor stars (Woosley & Weaver 1995). Observationally, silicon abundances are affected by contamination from CH and Hδ lines; departures from LTE do not seem to be a major concern, at least for Sun-like stars (Shi et al. 2008).

At the lowest metallicities, where the signature of low-Z SNeII is clearly seen, the [Si/Fe] ratio predicted by our GCE model may vary by up to 1 dex. Models 1 and 5, computed with Woosley & Weaver's (1995) case B and Kobayashi et al.'s (2006) $\varepsilon_{\rm HN} = 1$ yields for massive stars, respectively, predict a mildly declining trend of [Si/Fe] versus [Fe/H] over the whole metallicity interval covered by the observations [Fig. 14, panel a, short-dashed (red) and lower solid (black) lines, respectively]. The theoretical trend is in good agreement with the available data, apart from the flattening traced by observations at super-solar metallicities (Bensby et al. 2005), which might require a revision of current stellar yields from high-metallicity massive stars and/or SNeIa. A very steep decline of the [Si/Fe] ratio with metallicity in the $-4 <$ [Fe/H] < -1 metallicity range is obtained instead by assuming the yields of Kobayashi et al. (2006) with $\varepsilon_{\rm HN} = 0$ [Model 4, Fig. 14, panel a, upper solid (blue) line], at odds with observations. This would indicate that in the very early halo phases most massive stars must explode as HNe rather than normal SNeII.

Sulphur Like silicon, sulphur is an intermediate-mass element whose production is directly attributable to oxygen burning, either at the center or in the convective shells of massive stars, or during explosive nucleosynthesis (e.g. Woosley & Weaver 1995; Limongi & Chieffi 2003). As a volatile element, it is hardly affected by depletion onto dust particles, which makes it extremely useful in deciphering the chemical enrichment of damped Lyman α systems (see e.g. Nissen et al. 2004). Hence, unraveling the history of S enrichment in the early Galaxy has become a fundamental step towards our understanding of the high-redshift universe. However, sulphur abundance determinations in Galactic stars are currently highly debated. Takeda et al. (2005) find non-LTE abundance corrections to be negligible for the $\lambda\lambda$ 8693, 8694 Å S I lines of multiplet 6, while the $\lambda\lambda$ 9212, 9228, 9237 Å S I lines of multiplet 1 suffer significant negative non-LTE corrections (up to 0.2–0.3 dex). In the very metal-poor metallicity regime, a marked discordance is reported by Takeda et al. (2005) between the [S/Fe] values from the two abundance indicators: while the lines of multiplet 1 attain a nearly flat plateau (or even a slight downward bending), the lines of multiplet 6 show an ever-increasing trend with decreasing metallicity. A more recent analysis by Nissen et al. (2007), however, based on high S/N ratio spectra of 40 metal-poor halo stars, using both weak (λ 8694.6) and strong ($\lambda\lambda$ 9212.9, 9237.5) S I

lines, and taking non-LTE corrections into account, finds a flat trend of [S/Fe] versus [Fe/H] and no stars with [S/Fe] in excess of 0.60 dex.

In Fig. 14, panel b, the sulphur abundances measured by Nissen et al. (2007, crosses) are compared to the much more dispersed measurements by Caffau et al. (2005, triangles) from multiplets 1, 6 and 8. Disc data at higher metallicities are from Reddy et al. (2003, open squares). Also shown in Fig. 14, panel b, are the predictions of our GCE models for the evolution of [S/Fe] versus [Fe/H] (solid and dashed lines). Models 1 and 5, adopting the yields of Woosley & Weaver (1995) case B and Kobayashi et al. (2006) with $\varepsilon = 1$ for massive stars, respectively, favour a nearly flat trend of [S/Fe] versus [Fe/H] in the metallicity regime $-3 <$ [Fe/H] < -1. Model 4, instead, adopting the yields of Kobayashi et al. (2006) with $\varepsilon = 0$ for massive stars, predicts a steeply decreasing trend of [S/Fe] versus [Fe/H] in the same metallicity range. It is worth noticing that the outcome from Model 4 is at variance with observations if the data by Nissen et al. (2007) are used for comparison, but becomes compatible with the observations if the data from other authors (here Caffau et al. 2005) are added. Clearly, more data on S abundances in metal-poor stars are needed to reduce the current uncertainties in GCE modelling of S evolution, and to rule out the set(s) of stellar yields which produce results at variance with the observations.

Calcium The production of calcium is directly attributable to incomplete silicon and oxygen burning (Woosley & Weaver 1995). Departures from non-LTE in the line formation for both neutral and singly-ionized calcium have been recently investigated by Mashonkina et al. (2007), for a wide range of metallicities of the stars. As for Ca I, non-LTE abundance corrections depend on $T_{\rm eff}$, $\log g$, [Ca/H] and microturbulence value, and differ in value and sign for different Ca I lines. For Ca II, non-LTE leads to negative abundance corrections over the whole range of stellar parameters.

In Fig. 14, panel c, our model predictions on the behaviour of [Ca/Fe] as a function of [Fe/H] are compared to LTE abundances from Cayrel et al. (2004, stars), Lai et al. (2008, pentagons), Gratton et al. (2003, upside-down triangles), Reddy et al. (2003, 2006, squares) and Bensby et al. (2005, circles). The uncertainties in the model predictions for Ca are of the same order of magnitude as those for Si and S. At very low metallicities, Models 1 and 5 [short-dashed (red) line and lower solid (black) line, respectively] produce the best-fitting curves, whereas Model 4 [upper solid (blue) curve] overestimates the observed [Ca/Fe] ratios. None of the models is able to properly fit the thin-disc data.

Titanium The main isotope of titanium, ^{48}Ti, is produced mainly during complete and incomplete silicon burning. Spectroscopists may rely on several lines for deriving Ti abundances in stars. To our knowledge there is only one published non-LTE study of Ti in cool dwarfs and giants by Hauschildt et al. (1997); the data shown in Fig. 14, panel d, are all derived under the assumption of LTE.

As for K (see Sect. 4.2), also for Ti the theoretical predictions are offset with respect to the location of the data points in the [Ti/Fe] versus [Fe/H] diagram, though to a lesser extent (see Fig. 14, panel d). This clearly points to the need for a major revision of current SNII and HN yields, over the whole range of initial metallicities of the progenitor stars.

4.4. Iron-group elements

Scandium Scandium is produced in the innermost ejected layers of core-collapse SNe. It is made both as ^{45}Sc during neon burning and as the radioactive progenitor ^{45}Ti in explosive oxygen and silicon burning (Woosley & Weaver 1995). It is now widely recognized that artificially induced explosions in the progenitor star models lead to incorrect nucleosynthesis predictions, a consideration which more generally applies to the composition of the whole innermost ejecta (Fröhlich et al. 2006, and references therein). A quantity indispensable to correctly describe the nucleosynthesis in the innermost ejecta is the electron fraction in the layers undergoing explosive Si burning, Y_e. A value of Y_e in excess of 0.5 is obtained with a consistent treatment of neutrino interactions. This brings about large amounts of Sc, Ti and Zn (e.g. Fröhlich et al. 2006), thus solving the problem of their underproduction of the values observed in low-metallicity stars. Alternatively, an enhanced Sc production is obtained with a low-density model (Umeda & Nomoto 2005), where a weak jet expands the interior of the core-collapse SN progenitor before a strong jet develops, which explodes the star through a strong shock. Ti, Mg, Ca, Co and Zn production is enhanced in this model as well. The abundances of Sc, as well as Mn and Co, in the SN ejecta are then further enhanced by neutrino-nucleus interactions (the ν-process) occurring in Si-burning regions (Yoshida et al. 2008). Unfortunately, these studies do not provide complete grids of stellar yields useful for GCE models.

As a matter of fact, the predicted trend of [Sc/Fe] as a function of [Fe/H] severely disagrees with the [Sc/Fe] ratios measured in solar neighbourhood stars if the Kobayashi et al. (2006) yields for massive stars are used, independently of the assumed HN fraction (solid lines in Fig. 15, panel a). Marginal agreement between model predictions and observations is obtained by adopting the metallicity-dependent yields of Woosley & Weaver (1995, case B) for massive stars, but only for [Fe/H] < -1.5 [short-dashed (red) line in Fig. 15, panel a].

Vanadium Vanadium is synthesized mainly by incomplete explosive Si burning in massive stars (Limongi & Chieffi 2003).

The difficulty in measuring the V abundances in very metal-poor stars makes it troublesome to try and determine the trend of [V/Fe] versus [Fe/H] below [Fe/H] ≈ -1.5. It is clear though that current stellar yields underestimate the overall V abundance in the Galaxy, by at least 0.3–0.4 dex at disc metallicities (see Fig. 15, panel b).

Chromium Chromium is made chiefly during incomplete explosive Si burning (Woosley & Weaver 1995; Limongi & Chieffi 2003). Several authors (e.g. Honda et al. 2004; Lai et al. 2008; Bonifacio et al. 2009) have noticed that an offset exists between the abundances derived from Cr I and Cr II lines. Furthermore, an offset is found also between the abundances measured in giants and turnoff stars. The discrepancies may indicate non-LTE effects, unaccounted for in current analyses.

In Fig. 15, panel c, we display the predicted behaviour of [Cr/Fe] versus [Fe/H] (curves), together with the data from different authors (symbols). Model 5 [lower solid (black) line], including HN nucleosynthesis, is the one in better agreement with the observations. It favours the abundances derived from Cr II lines, rather than from Cr I, as indicative of the Cr content of halo stars (see also Kobayashi et al. 2006). Notice that Cr II lines can only be observed in giants.

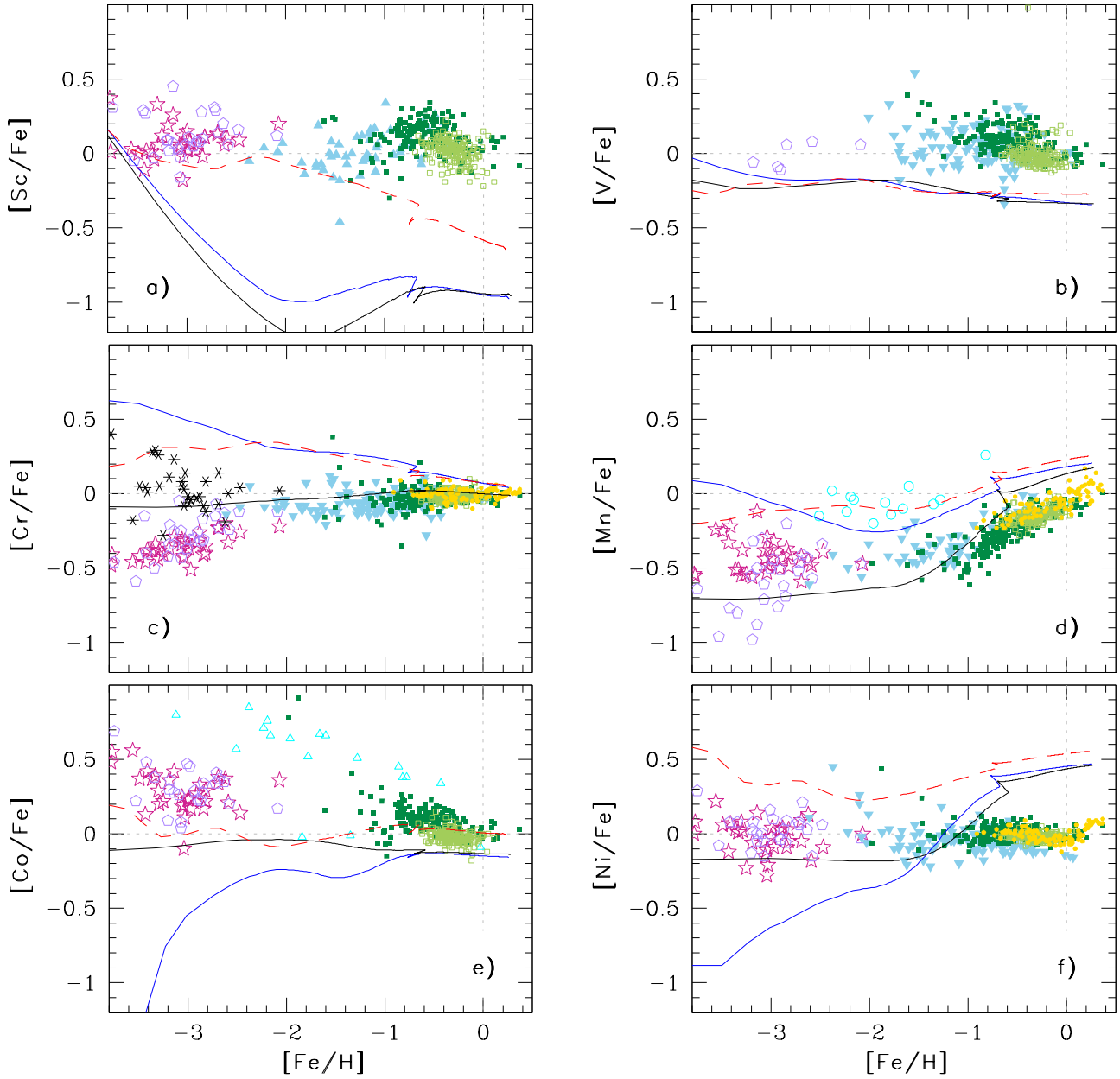

Fig. 15. Predicted behaviour of the relative ratios of several Fe-peak elements to iron (panel a: scandium, panel b: vanadium, panel c: chromium, panel d: manganese, panel e: cobalt, panel f: nickel) with respect to the relative iron abundance in the solar neighborhood, for Models 1 [short-dashed (red) lines], 4 [upper solid (blue) lines for Sc, V, Cr and Mn; lower solid (blue) lines for Co and Ni] and 5 [lower solid (black) lines for Sc, V, Cr and Mn; upper solid (black) lines for Co and Ni]. Also shown are data from Cayrel et al. (2004, stars), Lai et al. (2008, open pentagons), Bonifacio et al. (2009, asterisks, for Cr from Cr II lines, see text), Bergemann & Gehren (2008, open circles), Bergemann et al. (2010, open triangles), Gratton et al. (2003, upside-down triangles), Reddy et al. (2006, filled squares), Reddy et al. (2003, open squares), Bensby et al. (2005, filled circles, only for Cr and Ni) and Feltzing et al. (2007, filled circles, only for Mn). Bergemann & Gehren (2008) and Bergemann et al. (2010) performed non-LTE calculations; all the other abundance studies, instead, rely on the assumption of LTE. See the electronic edition of the journal for a colour version of this figure.

Manganese It is well established through theoretical modelling that manganese is mainly made in explosive silicon burning and nuclear statistical burning (e.g. Arnett 1996), but its yields from different types of SNe remain still uncertain. It is also debated whether or not the yields are metallicity dependent (Feltzing et al. 2007). Cescutti et al. (2008) have demonstrated that the evolution of Mn can be understood only if Mn yields from SNeIa are metallicity-dependent. This is a robust result, because it explains at the same time the evolution of Mn in the solar vicinity, the Galactic bulge and the Sagittarius dwarf spheroidal galaxy.

The Mn line at 602.1 nm is poorly reproduced by available hyper fine structure (HFS) linelist and should hence be discarded in careful abundance studies (Feltzing et al. 2007). Reddy et al.

(2006) include this line in their analysis, which may explain why they find similar trends of [Mn/Fe] versus [Fe/H] for their thick-disc and thin-disc samples, while Feltzing et al. (2007) find different trends below [Fe/H] = 0 (stars with kinematics typical of the thick disc show a steady increase of [Mn/Fe] with increasing [Fe/H], while stars with kinematics typical of the thin disc share almost the same [Mn/Fe] ratio). To our knowledge, there is only one work dealing with the important issue of non-LTE line formation for Mn (Bergemann & Gehren 2008). Though only 14 stars with [Fe/H] mostly from −1 to −2.5 are analyzed, there is intriguing circumstantial evidence that non-LTE corrections might run up to 0.5–0.7 dex at low metallicity (Fig. 15, panel d, open circles).

Let us now compare in Fig. 15, panel d, our model predictions on the behaviour of [Mn/Fe] as a function of [Fe/H] (solid and dashed lines) to the data obtained under the assumption of LTE by Cayrel et al. (2004, stars), Lai et al. (2008, open pentagons), Gratton et al. (2003, upside-down triangles), Reddy et al. (2003, 2006, squares) and Feltzing et al. (2007, filled circles). At the low metallicities typical of halo stars, say [Fe/H] < −1.5, the uncertainties in the GCE model predictions are very large, up to 0.8 dex. A model intermediate between Models 4 and 5 [upper (blue) and lower (black) solid lines, respectively], i.e. one allowing a significant fraction of high-mass stars to explode as HNe, can explain the observed [Mn/Fe] ratios very well. However, when considering the non-LTE corrections to the Mn abundances (Bergemann & Gehren 2008, open circles), the models without HNe (Models 1 and 4) better fit the data. At higher metallicities, and especially for [Fe/H] > −0.8, all the models fail to reproduce the observations. This is due to the abrupt rise of the [Mn/Fe] ratio predicted owing to the late, overwhelming contribution to Mn synthesis from SNeIa. Compelling evidence for a reduction of the global Mn yield from SNeIa is discussed in Cescutti et al. (2008, and references therein). However, we feel that full non-LTE analysis of larger samples of stars is badly needed before we can draw any firm conclusion about the chemical evolution of Mn.

Cobalt Cobalt is synthesized by complete Si burning in the deepest stellar layers, whereas Cr and Mn form in the outer incomplete Si-burning regions. Up to a few years ago, it was common wisdom that the [Co/Fe] ratio as measured in halo stars steady increases with decreasing metallicity for −4.0 < [Fe/H] < −2.5, whereas the [Cr/Fe] and [Mn/Fe] ratios decrease with decreasing [Fe/H] over the same metallicity range in the same objects. The difference in the observed trends was first explained by the mass-dependent mass cut in SNeII by Nakamura et al. (1999). Then, Umeda & Nomoto (2005) demonstrated that enhanced explosion energies may lead to higher Co and lower Cr and Mn production in low-metallicity, high-mass stars, in agreement with the observations. However, as mentioned in previous paragraphs, the usage of the Cr II lines to estimate Cr abundances in giant halo stars and the correction of Mn abundances for non-LTE effects have led to a radically different picture, in which Cr and Mn stay almost constant rather than decline towards the lowest metallicity end. At the same time, investigations of the influence of non-LTE and HFS splitting on the formation of Co lines and abundances in cool stars have resulted in a trend of increasing [Co/Fe] with decreasing [Fe/H] much steeper than thought before (Bergemann et al. 2010, open triangles in Fig. 15, panel e).

We have tried different prescriptions on the synthesis of Co in stars in the framework of our GCE model, but none of them has brought the model predictions into agreement with the relevant data (Fig. 15, panel e, solid and dashed lines). This is specially true if the non-LTE corrected values are used for comparison.

Nickel Nickel is mainly produced in the zones which undergo complete explosive Si burning in stars (e.g. Limongi & Chieffi 2003). Measurements of Ni in solar neighbourhood stars indicate a flat trend of [Ni/Fe] versus [Fe/H] over the whole metallicity range (Fig. 15, panel f, symbols).

None of our GCE models is able to explain the observed data (Fig. 15, panel f, solid and dashed curves). The uncertainties in the GCE model predictions are particularly severe at the lowest metallicities, where the signature of SNII nucleosynthesis clearly shows up. Partial agreement between theoretical predictions and observations is found with Model 5, adopting Kobayashi et al. (2006) yields for massive stars with $\varepsilon = 1$, but only in the low metallicity domain. The jump in [Ni/Fe] seen at [Fe/H] ∼ −1 is due to Ni production from SNeIa (see also Kobayashi et al. 2006). The Ni yield from SNeIa is a strong function of Y_e in the burning region, which, in turn, is determined by electron captures and, hence, is sensitive to uncertain quantities such as the propagation speed of the burning front and the central density of the white dwarf progenitor (Iwamoto et al. 1999). This leaves room for a downward revision of current Ni yields from SNeIa (Kobayashi et al. 2006).

Copper Romano & Matteucci (2007) have recently presented a comprehensive study of copper evolution in different systems. They have demonstrated that, on a galactic scale, Cu is mainly produced by massive stars, rather than by SNeIa as previously thought (Matteucci et al. 1993; Mishenina et al. 2002). In massive stars, Cu is made during core-helium and carbon-shell hydrostatic burnings, as well as in explosive complete Ne burning (e.g. Woosley & Weaver 1995; Limongi & Chieffi 2003).

In Fig. 16, panel a, we compare the predictions from Models 1 [short-dashed (red) line], 4 [solid (blue) line labelled 4] and 5 [solid (black) line labelled 5] to Cu data from a number of studies spanning the whole metallicity range from [Fe/H] ≈ −4 to [Fe/H] ≈ +0.5. In low-metallicity stars, Cu abundances are derived under the assumption of LTE from the near-UV lines of Cu I at 3247.53 and 3273.95 Å, taking the effects of HFS and isotopic splitting into account (Bihain et al. 2004; Lai et al. 2008). At higher metallicities, Cu abundances (Reddy et al. 2003, 2006) are obtained from LTE analysis of optical Cu I lines (5105.550, 5218.210 and 5220.090 Å); thorough consideration of the HFS and isotopic splitting is required for the 5105 Å line. As already pointed out by Romano & Matteucci (2007), the Cu content of extremely metal-poor stars is basically determined by explosive nucleosynthesis in massive stars, but as the metallicity grows, the contribution from the weak *s*-process operating in massive stars becomes increasingly important.

The uncertainties in modelling the Galactic evolution of Cu range from 0.9 dex at the lowest metallicities to 0.3 dex or even less above [Fe/H] = −2.5. Apparently, Model 1, adopting Woosley & Weaver (1995) case B yields for normal SNeII, provides the best fit to the observed [Cu/Fe] versus [Fe/H] trend for [Fe/H] > −2. At lower metallicities, a model intermediate between Models 4 and 5, accounting for a fraction of HNe, reproduces better the data. However, the reader should be aware that Cu formation through the main *s*-process acting in low-mass AGB stars has not been included in the models, following the

results of stellar nucleosynthesis studies that found it to be negligible (see Romano & Matteucci 2007, and references therein). We feel that, before drawing any firm conclusion on which yield set would be better for Cu, it would be worth re-investigating the issue of Cu production in LIMSs by means of updated AGB models. Low-metallicity intermediate-mass AGB stars could in principle produce enough Cu to affect the chemical evolution of this element. For example, a 5-$M_\odot$ AGB star with [Fe/H] ≈ -2.3 produces [Cu/Fe] ~ 1.0 dex. Cu is produced by neutrons released during convective thermal pulses by the ^{22}Ne(α, n)^{25}Mg reaction, similar to the weak *s*-process in massive stars. At present, yields of Cu from a full range of AGB masses and metallicities are not available to test this with a chemical evolution model.

Zinc Similarly to sulphur, zinc is seen in damped Lyman α systems where, due to its refractory behaviour, constitutes a sensible nucleosynthetic tracer (Nissen et al. 2004, and references therein). Observations of stars in the solar vicinity show that [Zn/Fe] is close to zero for metallicities in the interval $-2.0 <$ [Fe/H] $< +0.4$ (e.g. Bensby et al. 2005; Nissen et al. 2007), but rises steeply to [Zn/Fe] $\approx +0.5$ at the lowest metallicities (Cayrel et al. 2004). Such a trend is reinforced when non-LTE corrections are applied (Takeda et al. 2005). An extreme alpha-rich freezeout with $Y_e > 0.5$ is a practical mechanism to make zinc in high abundance from metal-poor SNeII (Fröhlich et al. 2006). An alternative possibility for high Zn/Fe production are Pop III core-collapse very massive ($m \sim 500$–1000 $M_\odot$) stars, in which, at the presupernova stage, silicon-burning regions occupy a large fraction, more than 20 per cent of the total mass (Ohkubo et al. 2006).

In Fig. 16, panel b, we compare the predictions from Models 1 [short-dashed (red) line], 4 and 5 (solid lines labelled 4 and 5, respectively) to LTE Zn abundances from several studies (symbols; see figure caption). Large uncertainties are associated to the model predictions at metallicities typical of the halo phase. None of the models is able to reproduce the observations: Model 1 is in qualitative agreement with the observed trend of increasing [Zn/Fe] with decreasing [Fe/H] in the metallicity interval $-4 <$ [Fe/H] < -1, but it underpredicts Zn. In contrast, the [Zn/Fe] versus [Fe/H] relation predicted by Model 5 for [Fe/H] < -1.5 is flat. Finally, Model 4 produces by far less Zn than required to explain the observations of this element in solar neighbourhood stars.

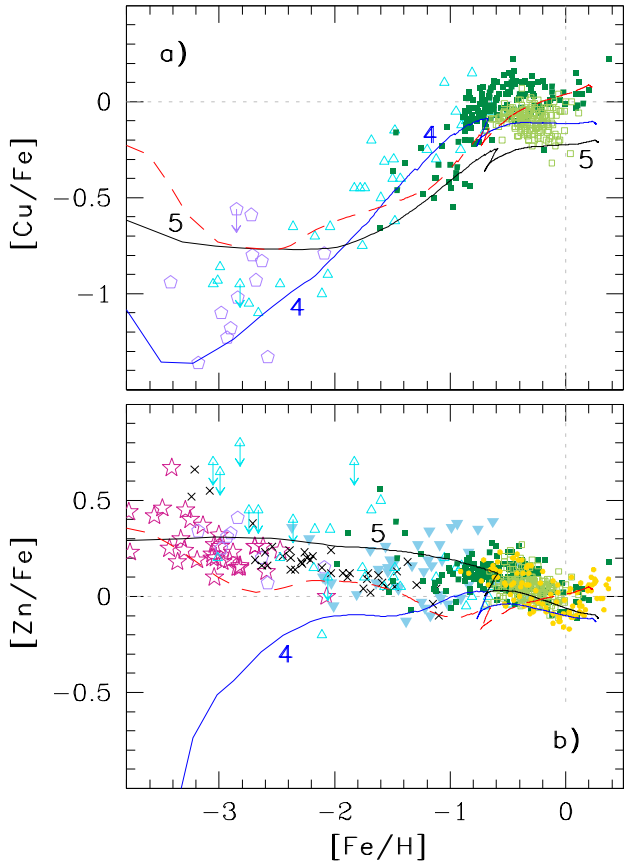

Fig. 16. [Cu/Fe] versus [Fe/H] (upper panel) and [Zn/Fe] versus [Fe/H] (lower panel) relations as predicted by Models 1 [short-dashed (red) lines], 4 and 5 (solid lines labelled 4 and 5, respectively) for the solar neighbourhood. Also shown are data from Cayrel et al. (2004, stars), Lai et al. (2008, open pentagons), Nissen et al. (2007, crosses), Bihain et al. (2004, open triangles), Gratton et al. (2003, upside-down triangles), Reddy et al. (2006, filled squares), Reddy et al. (2003, open squares) and Bensby et al. (2005, filled circles). See text for discussion.

5. The Galactic gradient

The distribution with Galactocentric distance of the abundances predicted by a GCE model depends not only on the adopted yields, but even more on the assumptions on the galactic parameters, star formation and infall laws and IMF. In particular, the slope of the gradients is strictly related to the radial variation of the star formation/infall rates, i.e. of the enrichment/dilution rates (e.g. Tosi 1988; Matteucci & François 1989). The yields, however, provide the absolute abundances and are therefore important ingredients for the gradients too.

The intriguing theme of the establishment and evolution of abundance gradients will be the subject of the next paper in this series. Here, for the sake of completeness we simply comment on the predicted present-day gradient for a few elements of interest. In Fig. 17, we show the present-day gradients of carbon, oxygen, sodium, magnesium, aluminium and silicon predicted by Models 1, 3, 4, 5, 9 and 15. For the comparison with the observations, we use the homogeneous data for nearly 200 classical Cepheid variable stars presented in a series of papers by S. Andrievsky and collaborators (Andrievsky et al. 2002a,b,c; Luck et al. 2003; Andrievsky et al. 2004; Kovtyukh et al. 2005; Luck et al. 2006).

It is clear that for some elements different choices of the yields do not provide only different *absolute abundances*, but also different *slopes* of the gradients. This is the case for carbon and oxygen, while a negligible effect is seen for the other elements, including elements heavier than Si, not shown in Fig. 17. It is worth noticing, in particular, that the models including mass loss and rotation in high-mass stars are the ones that better reproduce the slope of the present-day C gradient. As an example, in Fig. 17, panel a, we show the predictions of Model 9, using the Geneva group yields for rotating massive stars (upper dotted line). The theoretical curve is arbitrarily shifted by -0.5 dex (lower dotted line) to better compare the slope of the theoretical gradient with that of the gradient observed in Cepheids. Other models, using different nucleosynthesis prescriptions, predict a much flatter C gradient, at variance with observations. Model 3, using the older Maeder (1992) yields for solar-metallicity massive stars computed with high mass loss but no rotation, is in

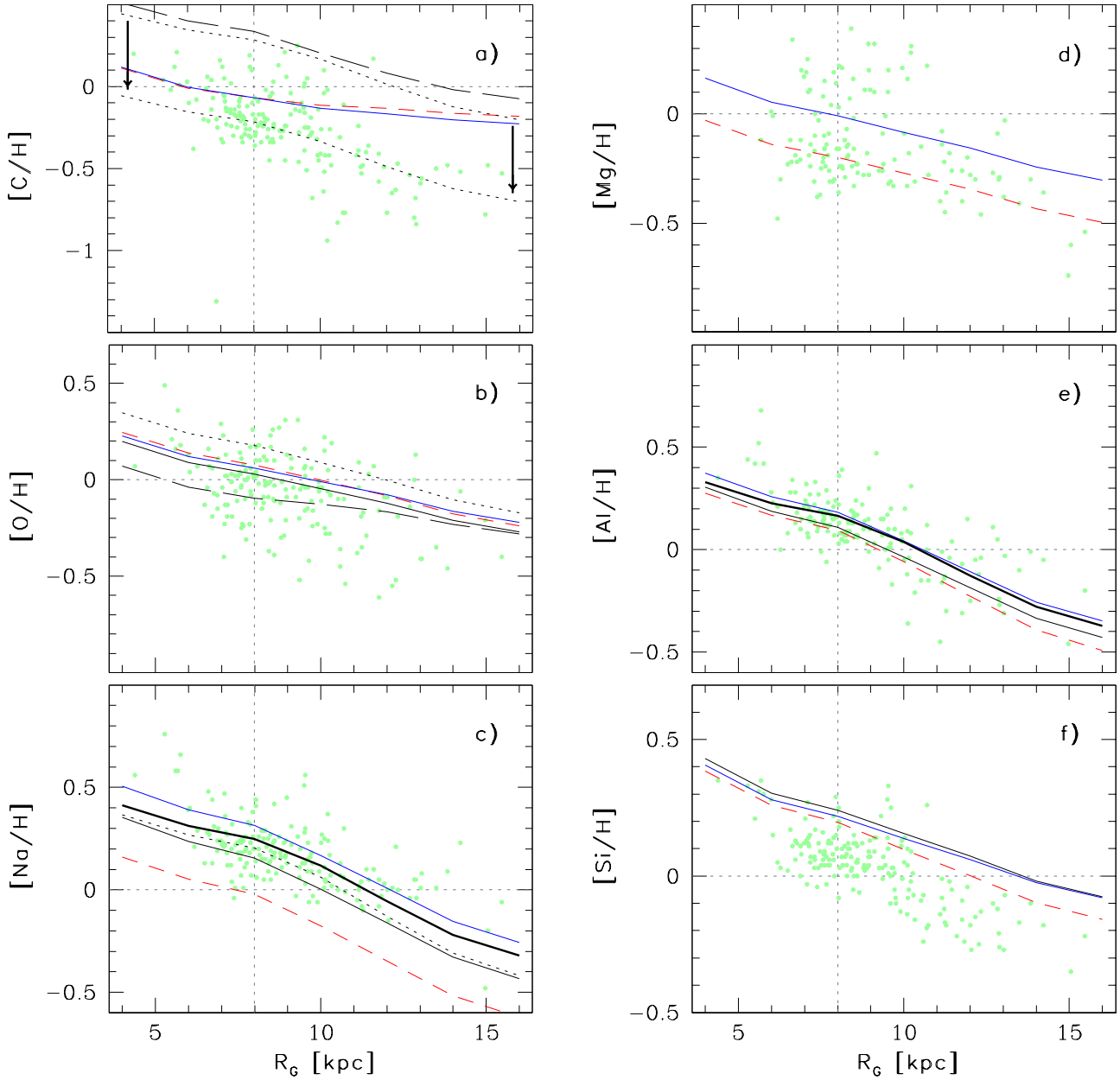

Fig. 17. Radial distribution of the abundances of carbon, oxygen, sodium, magnesium, aluminium and silicon in the disc of the Milky Way at the present time. The predictions from Models 1 [short-dashed (red) lines], 3 [long-dashed (black) lines, only for C and O], 4 [upper solid (blue) curves], 5 [lower solid (black) curves], 9 [dotted (black) lines, only for C, O and Na] and 15 (thick solid lines, only for Na and Al) are compared to the homogeneous data for Cepheid variable stars by Andrievsky et al. (2002a,b,c), Luck et al. (2003), Andrievsky et al. (2004), Kovtyukh et al. (2005) and Luck et al. (2006). In panels a and d the predictions from Model 5 are not shown because they are pretty much the same as Model 4. The intersection of the short-dashed vertical and horizontal (grey) lines in each panel marks the position of the Sun. See text for details. See the electronic edition of the journal for a colour version of this figure.

agreement with the slope of the observed C gradient, but produces a too flat O gradient [Fig. 17, panels a and b, long-dashed (black) lines].

There are basically two conditions that the models must meet to be judged in agreement with the observations. First, they have to pass slightly above the intercept of the dashed lines indicating the position of the Sun in each diagram. Second, they have to reproduce the slope of the observed gradient. The intersection of the vertical and horizontal dashed lines marks the position of the Sun in each panel. If the composition of the Sun is representative of the typical chemical enrichment occurring in the Galactic disc at a distance of $R_{\rm G} = R_{\rm G,\odot} = 8$ kpc from the Galactic centre, one expects the abundances of Cepheids at comparable Galactocentric distances to scatter slightly above the solar value, under the assumption that the metallicity of the ISM has only slightly evolved from the time of the Sun formation up to now (Tosi 1988). This is what is found for most elements, with the notable exceptions of carbon (on average lower than so-

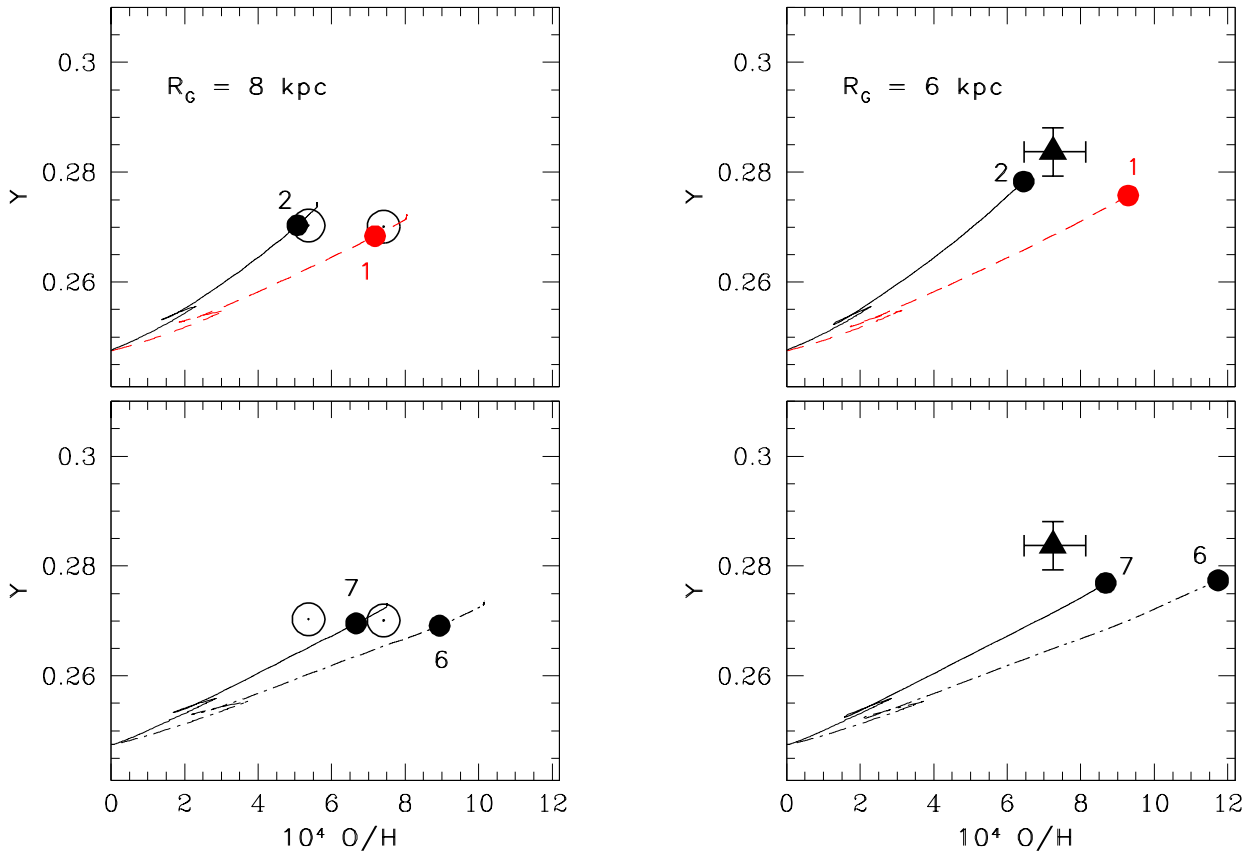

Fig. 18. Y versus 10^4 O/H in the solar vicinity (left panels) and in the inner disc (R_G = 6 kpc; right panels), as predicted by models with different nucleosynthesis prescriptions. Top panels: Model 1 [short-dashed (red) lines] versus Model 2 [solid (black) lines], showing the effect of changing the mass cut in models of SNII explosions. Bottom panels: Model 6 [dot-dashed (black) lines] versus Model 7 [solid (black) lines], with and without rotation in high-mass stars, respectively. Left panels: the filled circles on each theoretical track indicate the Y and 10^4 O/H values predicted at the time of the birth of the Sun, 4.5 Gyr ago. These are compared with the bulk (initial) abundances of He and O in the Sun (Sun symbols, from Grevesse & Sauval 1998 – higher O abundance – and Asplund et al. 2009 – lower O abundance). The effects of diffusion are taken into account in defining the protosolar abundances displayed in the figure (see the discussion in Asplund et al. 2009). Right panels: the final Y and 10^4 O/H values attained by the models are highlighted (filled circles) and compared to the abundances of He and O measured for M 17, an H II region located at 2.1 kpc distance from the Sun (filled triangles; see text for discussion).

lar in Cepheids, because of the occurrence of the first dredge-up; Kovtyukh et al. 2005), sodium and aluminium (on average enhanced with respect to solar, again reflecting evolutionary processes inside the stars themselves; Kovtyukh et al. 2005). While this may complicate the comparison with the absolute abundances of C, Na and Al predicted by the models, our conclusions on the slopes of the gradients should remain basically unaffected.

In conclusion, we have seen that, at least for some elements, the comparison of the gradients predicted by using different grids of yields with a homogeneous data set can prove useful to discriminate among different nucleosynthesis prescriptions.

6. The helium-to-heavy element enrichment ratio

In Figs. 18 to 20 we show the predicted behaviour of the helium mass fraction, Y, versus 10^4 O/H in the ISM for two Galactic radii, $R_G = R_{G,\odot}$ = 8 kpc (left panels) and R_G = 6 kpc (right panels). Shown are the predictions of models computed with different nucleosynthesis prescriptions (see Figs. 18 to 20 captions and detailed description of the adopted nucleosynthesis in Table 2).

The predictions of GCE models on the composition of the ISM in the solar vicinity 4.5 Gyr ago are usually compared, for elements heavier than He, to the photospheric solar abundances. However, this is incorrect, since the photospheric abundances are no longer representative of the original composition of the Sun at birth, because of the effects of diffusion (e.g. Bahcall et al. 2006). The solar abundances of He and O displayed in Figs. 18 to 20 for comparison with the theoretical model results (Sun symbols) have been corrected for the effects of diffusion (Asplund et al. 2009). We show both the values recommended by Grevesse & Sauval (1998), $Y_{\odot,\rm ini}$ = 0.2701, $\log\varepsilon(\rm O)_{\odot,\rm ini}$ = 8.87 [$\log\varepsilon(\rm O)_{\odot,\rm phot}$ = 8.83 ± 0.06], and those recommended by Asplund et al. (2009), $Y_{\odot,\rm ini}$ = 0.2703, $\log\varepsilon(\rm O)_{\odot,\rm ini}$ = 8.73 [$\log\varepsilon(\rm O)_{\odot,\rm phot}$ = 8.69 ± 0.05].

It can be immediately seen that the largest uncertainties in the model predictions are associated to the predicted oxygen abundances, while all the models predict virtually the same Y value at R_G = 8 kpc at Sun's birth and at R_G = 6 kpc at the present time. Small differences are found in the model predictions when changing the prescriptions on He and O synthesis

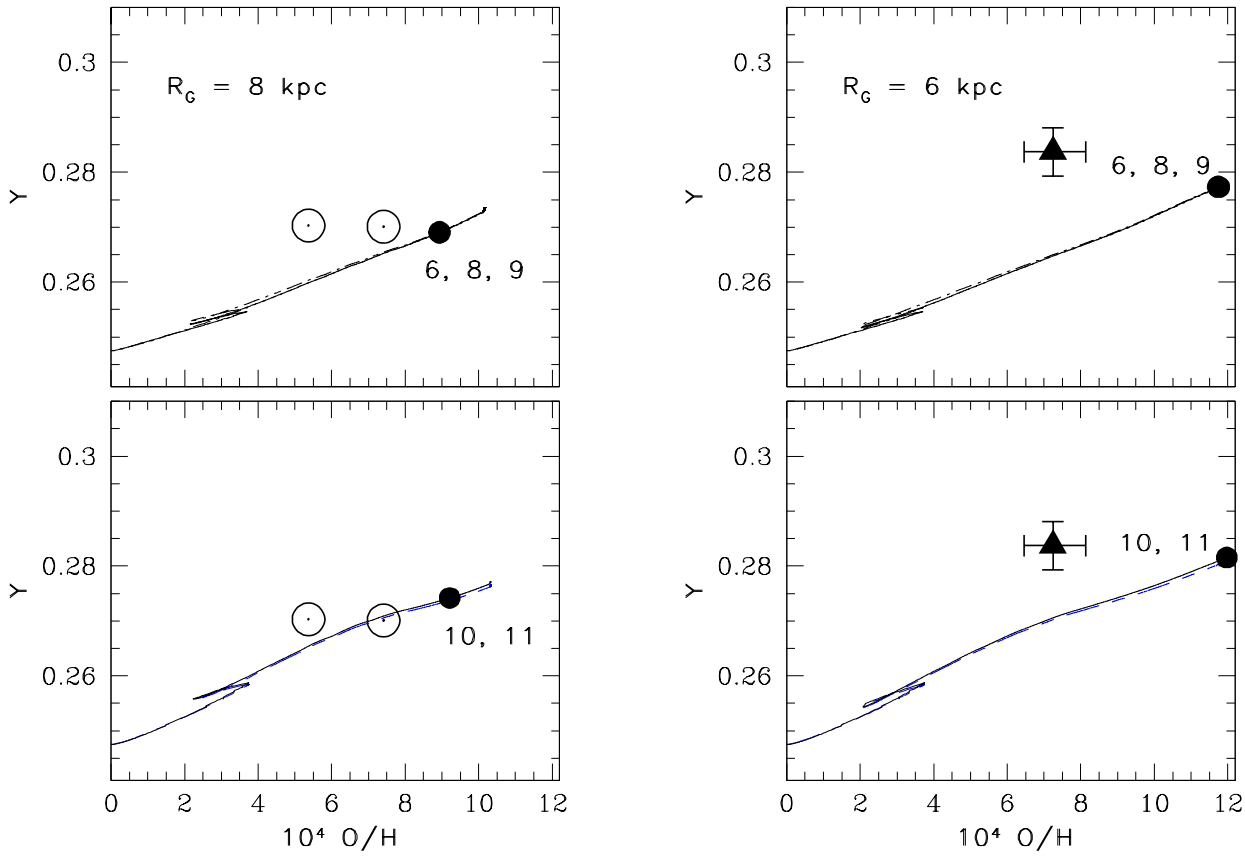

Fig. 19. Same as Fig. 18, but confronting the predictions from Models 6, 8 and 9 (upper panels; dot-dashed, solid and dotted lines, respectively) and 10 and 11 (lower panels; short-dashed-long-dashed and solid lines, respectively). The different model predictions overlap. This suggests that the uncertainties associated with the treatment of mass loss and HBB in AGB do not have an impact on the predicted Y versus 10^4 O/H behaviour.

in LIMSs (Fig. 19 and lower panels of Fig. 20). On the other hand, the differences become significant when changing the prescriptions on He and O synthesis in massive stars (Fig. 18 and upper panels of Fig. 20). In particular, the models adopting the yields by Hirschi et al. (2005) for solar-metallicity rotating massive stars (Models 6, 8, 9, 10, 11, 13 and 15) tend to overproduce oxygen in the Galaxy. In particular, the helium-to-metal enrichment ratio predicted by Model 13 around and above solar metallicity is $\Delta Y/\Delta Z \simeq 1$. This is barely consistent with the value of $\Delta Y/\Delta Z = 2.1 \pm 0.9$ suggested by Casagrande et al. (2007) for a large sample of nearby K dwarf stars. Models 3, 12 and 14 (the latter not shown in the figures), adopting the older yields by Maeder (1992) for solar-metallicity stars, instead, are consistent with $Y_{\odot,\,\rm ini} = 0.2703$, $\log\varepsilon(\rm O)_{\odot,\,\rm ini} = 8.73$, as suggested by Asplund et al. (2009), and give $\Delta Y/\Delta Z = 1.3$–1.5 for solar- and supersolar-metallicity stars, in good agreement with Casagrande et al.'s (2007) findings.

The best way to discriminate between the Hirschi et al. (2005) and Maeder (1992) yields for solar-metallicity stars is to compute the chemical evolution at inner radii where, owing to the higher metallicities attained, the differences in the model predictions are expected to exacerbate. In the inner Galaxy, at a distance of 2.1 ± 0.2 kpc from the Sun (Hoffmeister et al. 2008), lies M 17, the best Galactic H II region to derive He and O abundances, owing to the smallest correction for the presence of neutral helium (see Carigi & Peimbert 2008, and references therein). In Fig. 20, upper right panel, we compare the predictions from Models 1 and 3 for $R_{\rm G}$ = 6 kpc with the new determination of He and O abundances for M 17 by Carigi & Peimbert (2008). It is seen that the use of Maeder (1992) yields for solar-metallicity massive stars improves the model predictions. Independent chemical evolution studies have already supported Maeder (1992) yields for solar-metallicity massive stars (Giovagnoli & Tosi 1995; Carigi et al. 2005; Carigi & Peimbert 2008; McWilliam et al. 2008). On the other hand, it is worth noticing that also with the up-to-date yields computed by the Geneva group for *non-rotating* massive stars, the fits to the Y, O/H values at $R_{\rm G}$ = 8 kpc at Sun's birth and at $R_{\rm G}$ = 6 kpc at the present time improve with respect to the case with rotation (see Fig. 18, lower panels).

We deem it necessary to stress at this point that different assumptions about the model ingredients can change the conclusions. As an example, in Fig. 21 we show the results of Models 1S and 10S computed for $R_{\rm G}$ = 6 kpc (top panel) and $R_{\rm G}$ = 8 kpc (bottom panel), this time assuming a Scalo (1986) IMF. Because of the highest mass fraction per stellar generation locked up in stars that do not contribute to the chemical enrichment and because of the lower mass fraction falling in the 8–100 $M_\odot$ mass range according to this IMF, the models now produce less metals (and, hence, less oxygen) and less helium. Thus, while still consistent, within the uncertainties, with the initial He and O abundances in the Sun, they are by no means able

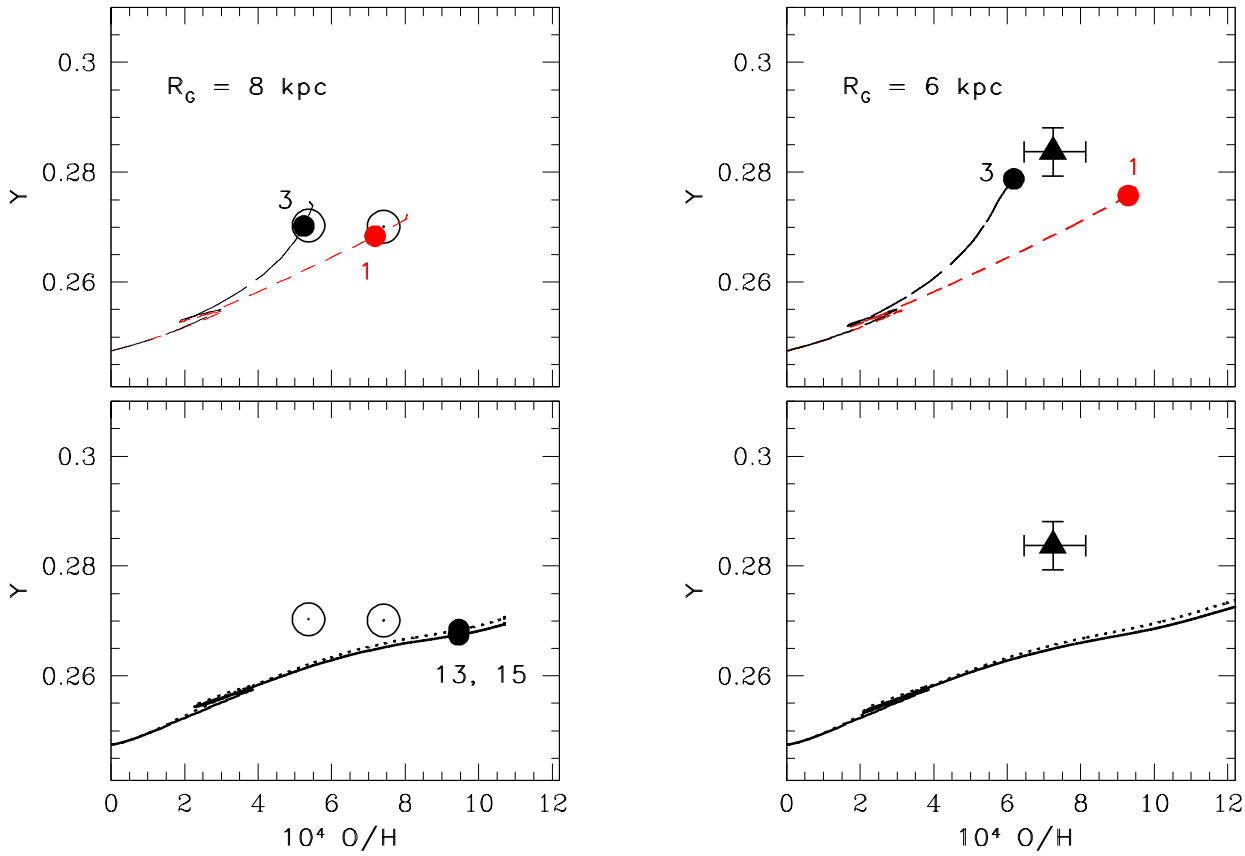

Fig. 20. Same as Fig. 18, but confronting the predictions from Models 1 and 3 [upper panels; short-dashed (red) and long-dashed (black) lines, respectively] and 13 and 15 (lower panels; thick dotted and thick solid lines, respectively).

to account for the abundances of He and O in M 17. Adopting different nucleosynthesis prescriptions would only worsen the discrepancy between model predictions and observations.

Finally, it is worth noticing that no constraints can be set at present on the helium-to-metal enrichment ratio in the solar neighbourhood at ages older than that of the Sun (Casagrande et al. 2007). This means that no constraints can be set on the He stellar yields for $Z < Z_{\odot}$ from chemical evolution studies of the Galaxy.

7. Summary and conclusions

In this paper, we have described the evolution of He and heavier elements from C to Zn in the Milky Way resulting from different sets of stellar yields and a well-tested chemical evolution model for the Galaxy.

In Sect. 2, we have provided a detailed comparison among different yield sets suitable for use in chemical evolution models of the Galaxy. We stress that the absence of a complete and homogeneous grid of stellar yields, computed with the same input physics for many initial masses and chemical compositions of the stars – say, from 0.8 $M_{\odot}$ to 100 $M_{\odot}$ and from zero to super-solar metallicity – is a major cause of uncertainty in the model predictions for elements such as He and N. In particular, detailed grids of yields for super-AGB stars are badly needed.

In Sect. 3, we introduced the adopted model for the chemical evolution of the Milky Way. This model well reproduces all the main observed features of the solar vicinity and of the whole Galactic disc. In particular, it is in agreement with the current star formation rate, gas and star radial density profiles and with the present-day Galactic SNII and SNIa rates and their ratio; it also reproduces the relative number of metal-poor-to-total stars, infall rate and degree of deuterium astration in the solar neighbourhood (see Chiappini et al. 2001; Romano et al. 2006, and Paper I). All these quantities are reproduced *independently of the choice of the stellar yields* and with a minimum number of free parameters, which justifies the use of the code to test possible stellar nucleosynthesis scenarios.

In Sects. 4 to 6, we described the model results, obtained by assuming different sets of stellar yields. In particular, in Sect. 4 we dealt with the behaviour of several abundance ratios as functions of metallicity in the solar neighbourhood. The radial abundance profiles were discussed in Sect. 5, whereas in Sect. 6 we focused on the relative helium-to-metal enrichment in the Galaxy. A meaningful comparison between model predictions and observations relies on carefully selected, reliable data sets. Hence, in Sects. 4 to 6, we also tried to ascertain the origin of possible inconsistencies on different data sets. We find that, in many cases, non-LTE and/or 3D analyses of stellar spectra lead to a profound revision of the abundance trends inferred by means of 1D, plane-parallel model atmospheres under the LTE approximation. This deeply impacts on the interpretation of the model results.

Despite several considerable improvements in the field of stellar evolution and nucleosynthesis in recent years, no single combination of stellar yields is found which is able to repro-

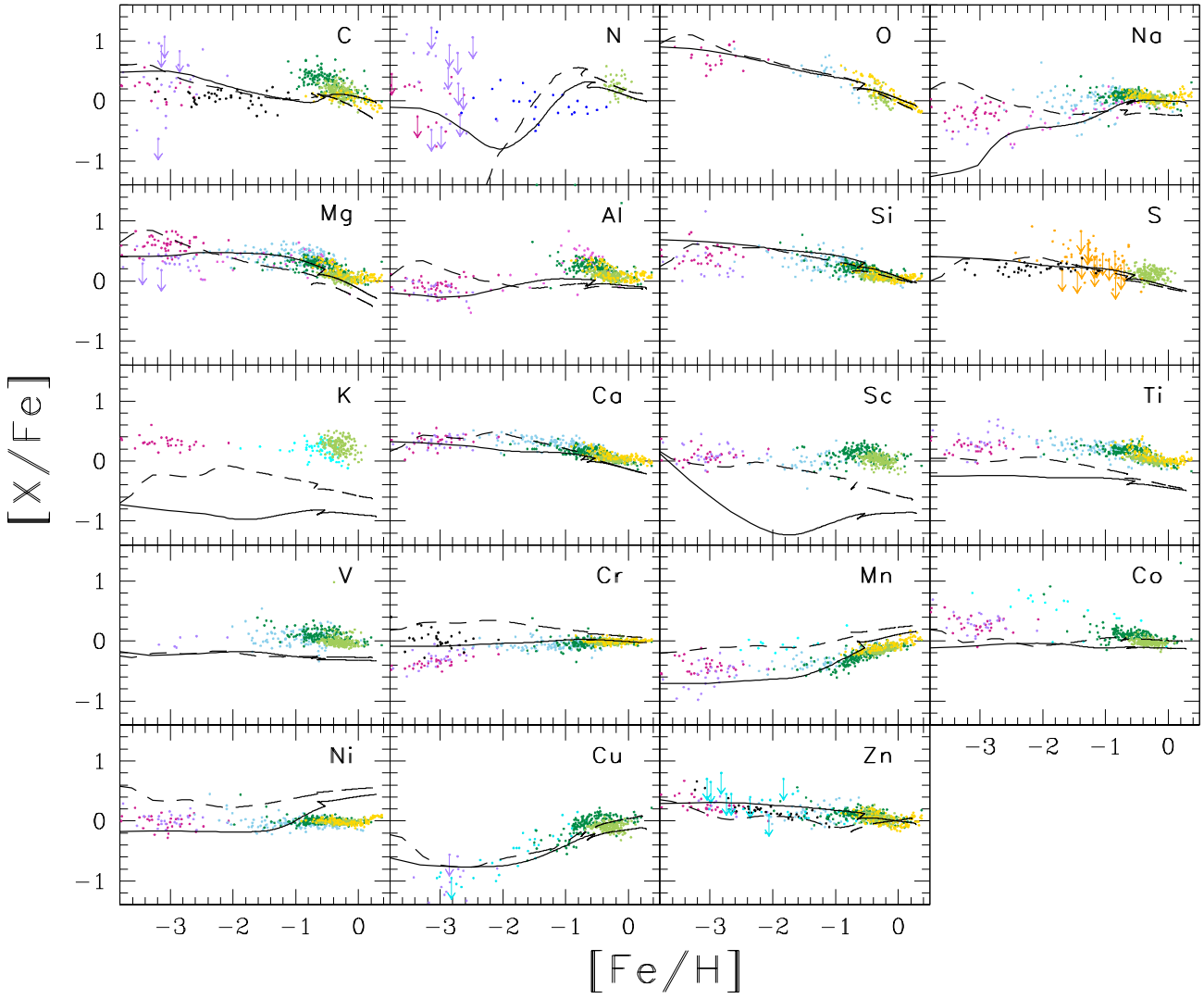

Fig. 22. [X/Fe] versus [Fe/H] relations for elements from C to Zn in the solar neighbourhood. The predictions from Models 1 and 15 (dashed and solid curves, respectively) are compared to data from several sources (see captions to Figs. 3 to 16 for references).

duce at once all the available measurements of chemical abundances and abundance ratios in the Milky Way. In Figs. 22 and 23, we summarize the results of our 'best yield choice', i.e. the combination of yields which maximizes the agreement with the largest number of observational constraints for the Milky Way. Our best model, Model 15 (solid lines in Figs. 22–23), uses the yields by Karakas (2010) for LIMSs, the pre-supernova yields of He and CNO elements by the Geneva group for massive stars, and the results of explosive nucleosynthesis of Kobayashi et al. (2006) for SNeII below 20 $M_{\odot}$ and HNe above that limit. For sake of comparison, we also show the results of Model 1 (dashed lines in Figs. 22–23), computed with the yields of van den Hoek & Groenewegen (1997) for LIMSs and Woosley & Weaver (1995) for massive stars. This is the combination of stellar yields most often used in the literature.

Model 15 fits better the behaviour of [C/Fe], [N/Fe], [Na/Fe], [Mg/Fe], [Al/Fe], [Cr/Fe] and, perhaps, [Zn/Fe] as a function of [Fe/H] in the solar neighbourhood, although some caveats still remain:

1. An exceptionally good fit between model predictions and observations of carbon in the disc is obtained if the carbon abundances are those based on the forbidden [C I] line at 872.7 nm (Bensby & Feltzing 2006, golden points in Fig. 22); otherwise, the fit is rather poor.
2. The overall trend of [N/Fe] versus [Fe/H] can not be satisfactorily explained by any model yet.
3. The behaviours of Na in halo stars and of Mg and Al at disc metallicities are still far from being understood. Rotation might strongly impact on yields of Na and Al from massive stars, but detailed computations suitable for use in GCE models of the Galaxy are still missing in the literature.

The evolution of oxygen in the solar neighbourhood and its solar abundance are very well reproduced by both models, thus indicating that its nucleosynthesis in stars is well understood by now. The same is true for Si, while S and Ca are slightly underestimated in the disc.

Potassium, scandium, titanium and vanadium are understimated by both models, with Model 15 performing worse for K, Sc and Ti. Ni is overestimated by Model 1, whereas Model 15 partially agrees with the data for halo stars.

Should future non-LTE analyses of larger samples of stars confirm the trends suggested by Bergemann & Gehren (2008)

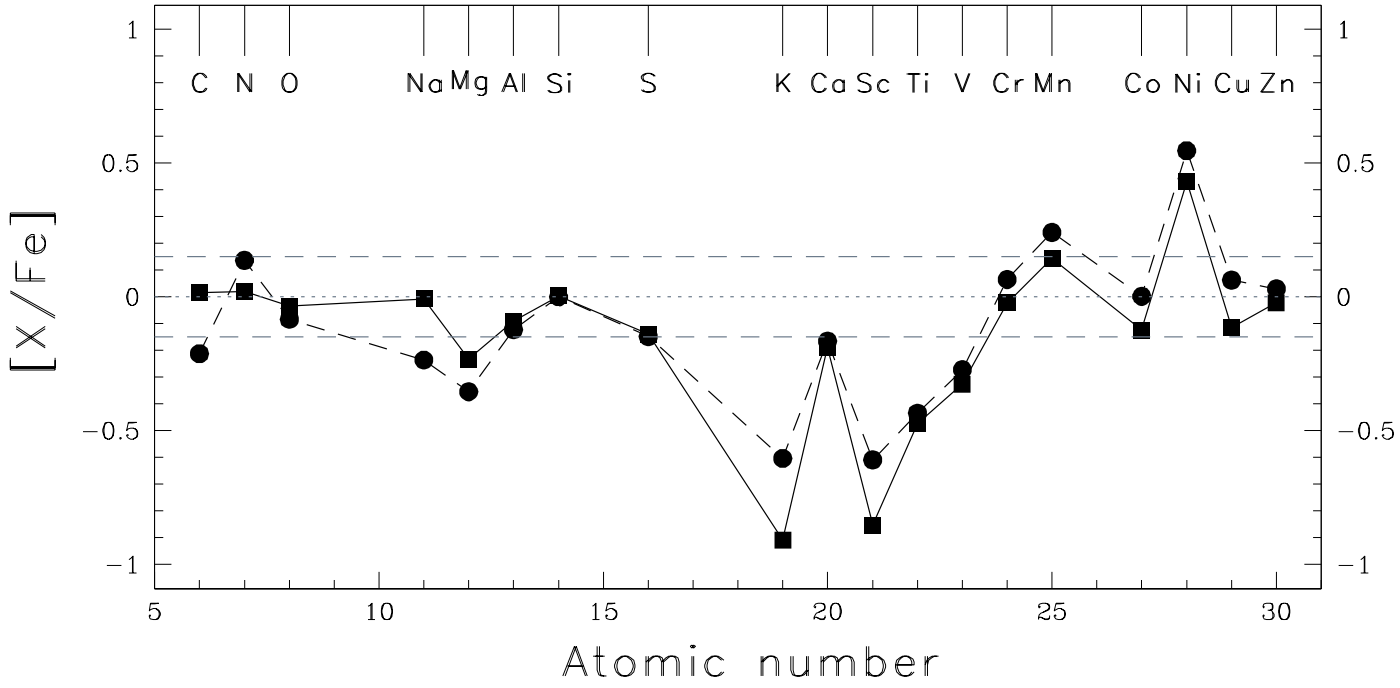

Fig. 23. [X/Fe] predicted by Model 1 (filled circles and dashed line) and Model 15 (filled squares and solid line) at Sun's birth for elements from C to Zn. The horizontal dotted line indicates the solar value of the ratios that the models must reproduce. The horizontal dashed lines allow for a ±0.15 dex error in the model predictions.

and Bergemann et al. (2010) for Mn and Co, respectively, we would be led to conclude that: (i) none of the models is able to explain the Co data in the Galaxy; (ii) Model 1 reproduces the halo data for Mn better than Model 15; (iii) neither model can explain the behaviour of Mn in the Galactic disc, most likely because of an excessive synthesis of Mn from SNeIa at late times. Indeed, as demonstrated by Cescutti et al. (2008), who studied Mn evolution in the solar neighbourhood, the Galactic bulge and the Sagittarius dwarf spheroidal galaxy, considering metallicity-dependent yields of Mn from SNeIa could provide a solution to the problem of the overproduction of Mn at late times.

Finally, Model 1 provides a very good fit to copper abundances measured in solar neighbourhood stars, while Model 15 fails to reproduce Cu abundances in disc stars. However, the role of AGB stars as Cu factories has still to be assessed, which may lead to improvements in Model 15 predictions for Cu at disc metallicities.

While exploding core-collapse SNe through an artificially induced piston or thermal bomb is acceptable for the external layers, only a correct treatment of the physics of the explosion could provide correct yields for the species produced in the innermost ejected layers, such as the Fe-peak nuclei. Our results are in agreement with recent claims that a correct treatment of the explosion physics is still missing in SN models.

The inclusion of rotation in high-mass stellar models has allowed to sensibly improve the predictions of GCE models on C evolution in the early Galaxy. Contrary to common wisdom, high N/O ratios at the lowest metallicities, instead, can be obtained even if not allowing for low-metallicity massive stars to rotate fast.

Yields for LIMSs computed by taking rotation into account are provided in the literature, but stopping the computations at the beginning of the TP-AGB stage makes them useless in GCE models, since the important effects of the TDU and HBB on the final yields are not considered.

We sincerely hope that the results of this study can trigger a further effort to improve and expand the current existing grids of stellar yields.

Acknowledgements. We thank the referee, Patrick François, for a thorough report which helped us to improve the presentation of the paper. Thanks are due to Monique Spite for providing the Cr II data for halo giants of the program "First Stars". DR and MT warmly thank Corinne Charbonnel for the many enlightening conversations. DR's research at Bologna University is supported by MIUR through grant PRIN 2007, prot. no. 2007JJC53X_001 (PI: F. Matteucci). DR and MT acknowledge the hospitality of the International Space Science Institute in Bern (CH) where some of the described issues have been discussed during Team meetings.

References

Akerman, C. J., Carigi, L., Nissen, P. E., Pettini, M., & Asplund, M. 2004, A&A, 414, 931
Andrievsky, S. M., Bersier, D., Kovtyukh, V. V., et al. 2002a, A&A, 384, 140
Andrievsky, S. M., Kovtyukh, V. V., Luck, R. E., et al. 2002b, A&A, 381, 32
Andrievsky, S. M., Kovtyukh, V. V., Luck, R. E., et al. 2002c, A&A, 392, 491
Andrievsky, S. M., Luck, R. E., Martin, P., & Lépine, J. R. D. 2004, A&A, 413, 159
Andrievsky, S. M., Spite, M., Korotin, S. A., et al. 2010, ArXiv e-prints
Andrievsky, S. M., Spite, M., Korotin, S. A., et al. 2007, A&A, 464, 1081
Andrievsky, S. M., Spite, M., Korotin, S. A., et al. 2008, A&A, 481, 481
Arnett, D. 1996, Supernovae and nucleosynthesis. An investigation of the history of matter, from the Big Bang to the present. (Princeton Univ. Press, Princeton)
Arnett, W. D. 1978, ApJ, 219, 1008
Asplund, M. 2005, ARA&A, 43, 481
Asplund, M., Grevesse, N., Sauval, A. J., & Scott, P. 2009, ARA&A, 47, 481
Bahcall, J. N., Serenelli, A. M., & Basu, S. 2006, ApJS, 165, 400
Baumüller, D., Butler, K., & Gehren, T. 1998, A&A, 338, 637
Baumüller, D. & Gehren, T. 1997, A&A, 325, 1088
Bensby, T. & Feltzing, S. 2006, MNRAS, 367, 1181
Bensby, T., Feltzing, S., & Lundström, I. 2003, A&A, 410, 527
Bensby, T., Feltzing, S., Lundström, I., & Ilyin, I. 2005, A&A, 433, 185

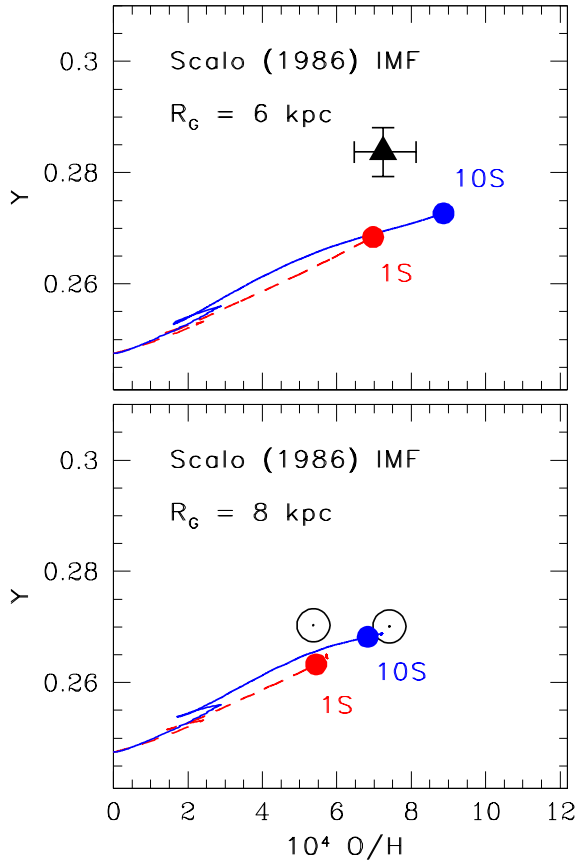

Fig. 21. Y versus 10^4 O/H predicted by models for the inner disc (R_G = 6 kpc; top panel) and for the solar vicinity (bottom panel) with different nucleosynthesis prescriptions [short-dashed (red) lines: Model 1S; solid (blue) lines: Model 10S]. The models adopt a Scalo (1986) IMF rather than a Kroupa et al. (1993) IMF. 'Observational' values for M 17 and the Sun are shown as well (see text).

Bergemann, M. & Gehren, T. 2008, A&A, 492, 823
Bergemann, M., Pickering, J. C., & Gehren, T. 2010, MNRAS, 401, 1334
Bihain, G., Israelian, G., Rebolo, R., Bonifacio, P., & Molaro, P. 2004, A&A, 423, 777
Bonifacio, P., Spite, M., Cayrel, R., et al. 2009, A&A, 501, 519
Boothroyd, A. I. & Sackmann, I. 1988, ApJ, 328, 653
Caffau, E., Bonifacio, P., Faraggiana, R., et al. 2005, A&A, 441, 533
Carigi, L. & Peimbert, M. 2008, Revista Mexicana de Astronomia y Astrofisica, 44, 341
Carigi, L., Peimbert, M., Esteban, C., & García-Rojas, J. 2005, ApJ, 623, 213
Casagrande, L., Flynn, C., Portinari, L., Girardi, L., & Jimenez, R. 2007, MNRAS, 382, 1516
Cayrel, R., Depagne, E., Spite, M., et al. 2004, A&A, 416, 1117
Cescutti, G., Matteucci, F., Lanfranchi, G. A., & McWilliam, A. 2008, A&A, 491, 401
Cescutti, G., Matteucci, F., McWilliam, A., & Chiappini, C. 2009, A&A, 505, 605
Chiappini, C., Hirschi, R., Meynet, G., et al. 2006, A&A, 449, L27
Chiappini, C., Matteucci, F., & Gratton, R. 1997, ApJ, 477, 765
Chiappini, C., Matteucci, F., & Romano, D. 2001, ApJ, 554, 1044
Chiappini, C., Romano, D., & Matteucci, F. 2003, MNRAS, 339, 63
Chieffi, A. & Limongi, M. 2004, ApJ, 608, 405
Chiosi, C. & Caimmi, R. 1979, A&A, 80, 234
Clayton, D. D. 1983, Principles of stellar evolution and nucleosynthesis. (Univ. of Chicago Press, Chicago)
Clayton, D. D. 2003, Handbook of Isotopes in the Cosmos (Cambridge Univ. Press, Cambridge)
de Jager, C., Nieuwenhuijzen, H., & van der Hucht, K. A. 1988, A&AS, 72, 259
Decressin, T., Meynet, G., Charbonnel, C., Prantzos, N., & Ekström, S. 2007, A&A, 464, 1029
Dray, L. M. & Tout, C. A. 2003, MNRAS, 341, 299
Dray, L. M., Tout, C. A., Karakas, A. I., & Lattanzio, J. C. 2003, MNRAS, 338, 973
Edmunds, M. G. & Pagel, B. E. J. 1978, MNRAS, 185, 77
Edvardsson, B., Andersen, J., Gustafsson, B., et al. 1993, A&A, 275, 101
Ekström, S., Meynet, G., Chiappini, C., Hirschi, R., & Maeder, A. 2008, A&A, 489, 685
Fabbian, D., Nissen, P. E., Asplund, M., Pettini, M., & Akerman, C. 2009, A&A, 500, 1143
Feltzing, S., Fohlman, M., & Bensby, T. 2007, A&A, 467, 665
François, P., Matteucci, F., Cayrel, R., et al. 2004, A&A, 421, 613
Fröhlich, C., Hauser, P., Liebendörfer, M., et al. 2006, ApJ, 637, 415
Gehren, T., Shi, J. R., Zhang, H. W., Zhao, G., & Korn, A. J. 2006, A&A, 451, 1065
Giovagnoli, A. & Tosi, M. 1995, MNRAS, 273, 499
Girardi, L., Bressan, A., Bertelli, G., & Chiosi, C. 2000, A&AS, 141, 371
Goswami, A. & Prantzos, N. 2000, A&A, 359, 191
Gratton, R. G., Carretta, E., Claudi, R., Lucatello, S., & Barbieri, M. 2003, A&A, 404, 187
Grevesse, N. & Sauval, A. J. 1998, Space Science Reviews, 85, 161
Groenewegen, M. A. T. & de Jong, T. 1993, A&A, 267, 410
Hauschildt, P. H., Allard, F., Alexander, D. R., & Baron, E. 1997, ApJ, 488, 428
Henry, R. B. C., Edmunds, M. G., & Köppen, J. 2000, ApJ, 541, 660
Hirschi, R. 2005, in IAU Symposium, Vol. 228, From Lithium to Uranium: Elemental Tracers of Early Cosmic Evolution, ed. V. Hill, P. François, & F. Primas, 331
Hirschi, R. 2007, A&A, 461, 571
Hirschi, R., Meynet, G., & Maeder, A. 2005, A&A, 433, 1013
Hoffmeister, V. H., Chini, R., Scheyda, C. M., et al. 2008, ApJ, 686, 310
Honda, S., Aoki, W., Kajino, T., et al. 2004, ApJ, 607, 474
Iben, Jr., I. & Truran, J. W. 1978, ApJ, 220, 980
Israelian, G., Ecuvillon, A., Rebolo, R., et al. 2004, A&A, 421, 649
Ivanova, D. V. & Shimanskiĭ, V. V. 2000, Astronomy Reports, 44, 376
Iwamoto, K., Brachwitz, F., Nomoto, K., et al. 1999, ApJS, 125, 439
Iwamoto, K., Mazzali, P. A., Nomoto, K., et al. 1998, Nature, 395, 672
Izzard, R. G., Tout, C. A., Karakas, A. I., & Pols, O. R. 2004, MNRAS, 350, 407
Karakas, A. & Lattanzio, J. C. 2007, PASA, 24, 103
Karakas, A. I. 2010, MNRAS, 403, 1413
Karakas, A. I., Lattanzio, J. C., & Pols, O. R. 2002, PASA, 19, 515
Karakas, A. I., van Raai, M. A., Lugaro, M., Sterling, N. C., & Dinerstein, H. L. 2009, ApJ, 690, 1130
Kobayashi, C., Umeda, H., Nomoto, K., Tominaga, N., & Ohkubo, T. 2006, ApJ, 653, 1145
Kovtyukh, V. V., Wallerstein, G., & Andrievsky, S. M. 2005, PASP, 117, 1173
Kroupa, P., Tout, C. A., & Gilmore, G. 1993, MNRAS, 262, 545
Kudritzki, R. P., Pauldrach, A., Puls, J., & Abbott, D. C. 1989, A&A, 219, 205
Lai, D. K., Bolte, M., Johnson, J. A., et al. 2008, ApJ, 681, 1524
Limongi, M. & Chieffi, A. 2003, ApJ, 592, 404
Luck, R. E., Gieren, W. P., Andrievsky, S. M., et al. 2003, A&A, 401, 939
Luck, R. E., Kovtyukh, V. V., & Andrievsky, S. M. 2006, AJ, 132, 902
Maeder, A. 1992, A&A, 264, 105
Marcolini, A., Gibson, B. K., Karakas, A. I., & Sánchez-Blázquez, P. 2009, MNRAS, 395, 719
Marigo, P. 2001, A&A, 370, 194
Marigo, P., Girardi, L., & Bressan, A. 1999, A&A, 344, 123
Mashonkina, L., Korn, A. J., & Przybilla, N. 2007, A&A, 461, 261
Matteucci, F. 1986, MNRAS, 221, 911
Matteucci, F. & François, P. 1989, MNRAS, 239, 885
Matteucci, F. & Greggio, L. 1986, A&A, 154, 279
Matteucci, F., Raiteri, C. M., Busso, M., Gallino, R., & Gratton, R. 1993, A&A, 272, 421
McWilliam, A., Matteucci, F., Ballero, S., et al. 2008, AJ, 136, 367
Meynet, G., Chiappini, C., Georgy, C., et al. 2009, in IAU Symposium, Vol. 254, The Galaxy Disk in Cosmological Context, ed. J. Andersen, J. Bland-Hawthorn, & B. Nordström (Cambridge Univ. Press), 325
Meynet, G. & Maeder, A. 2002a, A&A, 390, 561
Meynet, G. & Maeder, A. 2002b, A&A, 381, L25
Mishenina, T. V., Kovtyukh, V. V., Soubiran, C., Travaglio, C., & Busso, M. 2002, A&A, 396, 189
Nakamura, T., Umeda, H., Nomoto, K., Thielemann, F.-K., & Burrows, A. 1999, ApJ, 517, 193
Nissen, P. E., Akerman, C., Asplund, M., et al. 2007, A&A, 469, 319
Nissen, P. E., Chen, Y. Q., Asplund, M., & Pettini, M. 2004, A&A, 415, 993
Nissen, P. E., Primas, F., Asplund, M., & Lambert, D. L. 2002, A&A, 390, 235
Nomoto, K., Thielemann, F., & Wheeler, J. C. 1984, ApJ, 279, L23
Ohkubo, T., Umeda, H., Maeda, K., et al. 2006, ApJ, 645, 1352

Portinari, L., Chiosi, C., & Bressan, A. 1998, A&A, 334, 505
Pumo, M. L., D'Antona, F., & Ventura, P. 2008, ApJ, 672, L25
Ramírez, I., Allende Prieto, C., & Lambert, D. L. 2007, A&A, 465, 271
Reddy, B. E., Lambert, D. L., & Allende Prieto, C. 2006, MNRAS, 367, 1329
Reddy, B. E., Tomkin, J., Lambert, D. L., & Allende Prieto, C. 2003, MNRAS, 340, 304
Reimers, D. 1975, Mémoires de la Société Royale des Sciences de Liège, 8, 369
Renzini, A. & Voli, M. 1981, A&A, 94, 175
Romano, D., Chiappini, C., Matteucci, F., & Tosi, M. 2005, A&A, 430, 491 (Paper I)
Romano, D. & Matteucci, F. 2007, MNRAS, 378, L59
Romano, D., Matteucci, F., Salucci, P., & Chiappini, C. 2000, ApJ, 539, 235
Romano, D., Tosi, M., Chiappini, C., & Matteucci, F. 2006, MNRAS, 369, 295
Russell, S. C. & Dopita, M. A. 1992, ApJ, 384, 508
Scalo, J. M. 1986, Fundamentals of Cosmic Physics, 11, 1
Schaller, G., Schaerer, D., Meynet, G., & Maeder, A. 1992, A&AS, 96, 269
Shi, J. R., Gehren, T., Butler, K., Mashonkina, L. I., & Zhao, G. 2008, A&A, 486, 303
Shi, J. R., Gehren, T., & Zhao, G. 2004, A&A, 423, 683
Siess, L. 2007, A&A, 476, 893
Spite, M., Cayrel, R., Plez, B., et al. 2005, A&A, 430, 655
Straniero, O., Chieffi, A., Limongi, M., et al. 1997, ApJ, 478, 332
Takeda, Y., Hashimoto, O., Taguchi, H., et al. 2005, PASJ, 57, 751
Timmes, F. X., Woosley, S. E., & Weaver, T. A. 1995, ApJS, 98, 617
Tinsley, B. M. 1979, ApJ, 229, 1046
Tinsley, B. M. 1980, Fundamentals of Cosmic Physics, 5, 287
Tosi, M. 1988, A&A, 197, 33
Tosi, M. 2007, in ASP Conf. Ser., Vol. 378, Why Galaxies Care About AGB Stars: Their Importance as Actors and Probes, ed. F. Kerschbaum, C. Charbonnel, & R. F. Wing, 353
Umeda, H. & Nomoto, K. 2002, ApJ, 565, 385
Umeda, H. & Nomoto, K. 2005, ApJ, 619, 427
van den Hoek, L. B. & Groenewegen, M. A. T. 1997, A&AS, 123, 305
Vassiliadis, E. & Wood, P. R. 1993, ApJ, 413, 641
Ventura, P. & D'Antona, F. 2008a, MNRAS, 385, 2034
Ventura, P. & D'Antona, F. 2008b, A&A, 479, 805
Wallerstein, G., Iben, I. J., Parker, P., et al. 1997, Reviews of Modern Physics, 69, 995
Woosley, S. E. & Weaver, T. A. 1995, ApJS, 101, 181
Yoshida, T., Umeda, H., & Nomoto, K. 2008, ApJ, 672, 1043
Zhang, H. W., Gehren, T., Butler, K., Shi, J. R., & Zhao, G. 2006, A&A, 457, 645